Annu. Rev. Nucl. Part. Sci. 1999. 49:217–53

HIGH-ENERGY HADRON-INDUCED DILEPTON PRODUCTION FROM NUCLEONS AND NUCLEI

P. L. McGaughey, J. M. Moss, and J. C. Peng
Los Alamos National Laboratory, Los Alamos, New Mexico 87545;
e-mail: plm@lanl.gov, jmm@lanl.gov, peng@lanl.gov

Key Words Drell-Yan, nuclear dependence, quarkonium

■ **Abstract** We review the production of high-mass lepton pairs in fixed-target experiments, including both Drell-Yan (DY) and heavy quarkonium production [J/ψ, ψ', $\Upsilon(1S)$, $\Upsilon(2S)$, and $\Upsilon(3S)$]. In recent years, DY data have become standard input to the determination of parton density distributions. DY data have recently yielded the first measurement of the x dependence of the $\bar{d}/\bar{u}$ asymmetry of the proton. Similar to the observations in deeply inelastic scattering, precision measurements of the nuclear dependence of the proton-induced DY process exhibit shadowing at small target momentum fraction, x_2. There is, however, no evidence of enhanced DY production from nuclear targets. Mean transverse momenta of DY pairs are observed to increase with target mass. These data, analyzed within a new theoretical framework, provide an estimation of the energy loss of fast quarks in nuclear matter. In contrast to the DY process, there are large nuclear effects in the production of all quarkonia. These effects show strong dependence on p_t and x_F but do not scale with x_2. Statistically less precise measurements of D meson (open-charm) production at small x_F are consistent with no nuclear dependence.

CONTENTS

0163-8998/99/1201-0217$08.00

1. INTRODUCTION

The experimental detection of high-mass[1] lepton pairs produced in hadronic reactions has a long and rich history. The famous quarkonium states that revealed the existence of the charm and beauty quarks in the 1970s were discovered through their dilepton decay branches. They are superimposed on a continuum, which was anticipated theoretically in 1970 (1) and is now known as the Drell-Yan (DY) process (Figure 1). The DY process, electromagnetic quark-antiquark annihilation, is shown diagramatically in Figure 2, along with its close relative, deeply inelastic lepton scattering (DIS). By 1980, DY production was already a source of information about antiquark structure of the nucleon. Additionally, DY production with beams of pions and kaons yielded the structure functions of these unstable particles for the first time. Also notable in the history of the DY process were the discoveries of the $W^{\pm}$ and Z^0 particles in 1983, produced by a generalized (vector boson exchange) quark-antiquark annihilation mechanism.

In the mid-1980s some nagging theoretical issues were resolved, with the result that by the 1990s the DY process had joined DIS as a source of quantitative information on the quark structure of hadrons. Because the DY process at leading order explicitly involves one antiquark, it provides a sensitive measurement of antiquark structure even in kinematic regions where quarks dominate in number.

The peaks in Figure 1 are interlopers in an otherwise well-understood spectrum. They are seen along with the DY pairs because the $^3S_1$ states of heavy quarkonium have substantial decay branches to dileptons. However, the production of heavy quarkonium is a strong interaction process. At beam energies well above threshold, gluon fusion is the dominant production mechanism. Unlike the well-characterized DY process, the theoretical description of quarkonium production at the low transverse momenta (p_t) characteristic of fixed-target experiments requires a number of model-dependent assumptions (3).

Although the production mechanisms of quarkonia and the DY continuum differ greatly, these two types of processes are often reviewed together (4–7) because the data come from the same experiments. We continue that tradition here. The main

[1]In the context of this review, high mass is $M_{l^+l^-} \geq M_{J/\psi}$.

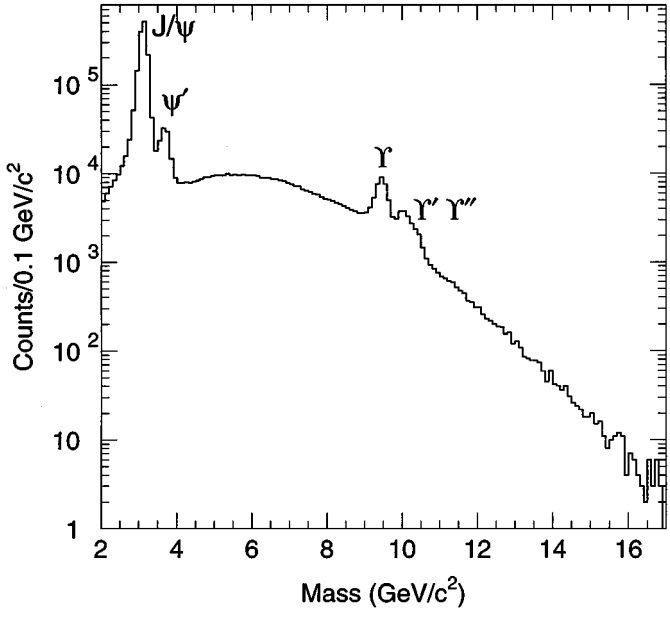

Figure 1 Combined dimuon mass spectrum from Fermilab E866 (2): p + p and p + d collisions at 800 GeV/c. The shape of the continuum results from the mass dependence of the Drell-Yan process folded with the acceptance of the spectrometer.

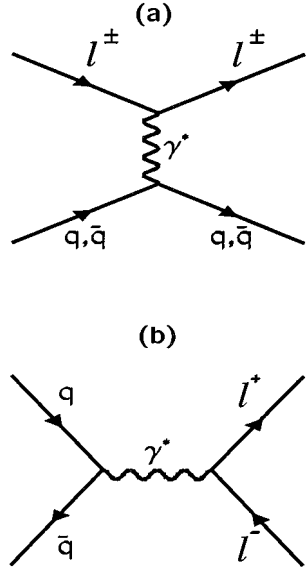

Figure 2 Feynman graphs for the electromagnetic processes (*a*) deeply inelastic lepton scattering and (*b*) the Drell-Yan process.

emphasis of this review is the application of dilepton production as a tool to investigate particular physics topics. New experimental work has been carried out in recent years by few but prolific collaborations working in the fixed-target programs at the CERN Super Proton Synchrotron (SPS) accelerator and at Fermilab. This review concentrates on new experimental results published after the comprehensive review of Freudenreich (7).

Lepton-pair production forms a major thrust of the collider program at Fermilab. We review those results only as they pertain directly to the physics addressed by the fixed-target experiments.

Section 2 presents an overview of the DY process, highlighting significant developments in theory and experiment. Sections 3.1 through 3.4 present recent and future applications of the DY process to the study of the quark structure of hadrons. In the remainder of Section 3, we discuss several physics topics related to the nuclear dependence of the DY process. Section 4 reviews the status of quarkonium and open heavy-flavor production in nuclei and their relation to quarkonium suppression as a signal for the formation of the quark-gluon plasma (QGP) in high-energy collisions of heavy ions. Finally, in Section 5, we look at some of the near-future opportunities in dilepton physics.

2. THE DRELL-YAN PROCESS

2.1 Drell-Yan Process in the Parton Model

The parton model expression for the DY process conveys the essential simplicity of the reaction.

$$\frac{d^2\sigma}{dM^2 dx_F} = \frac{4\pi\alpha^2}{9M^2 s}\frac{1}{(x_1+x_2)}\sum_a e_a^2[q_a(x_1)\bar{q}_a(x_2)+\bar{q}_a(x_1)q_a(x_2)]. \qquad 1.$$

Here $q_a(x)$ are the quark or antiquark structure functions of the two colliding hadrons evaluated at momentum fractions x_1 and x_2. The sum is over quark flavors. In addition, one has the kinematic relations,

$$\begin{aligned} \tau &\equiv x_1 x_2 = M^2/s, \\ x_F &= x_1 - x_2, \end{aligned} \qquad 2.$$

where M is the invariant mass of the lepton pair and s is the square of the center-of-mass energy. The cross section is proportional to α^2, indicating its electromagnetic character. The parton-model scaling properties of the DY process are illustrated in Figure 3, which shows data from experiments at 400 GeV/c (8) and at 800 GeV/c (9, 10; PL McGaughey et al, unpublished data). In the parton model, the angular distribution of dileptons is characteristic of the decay of a transversely polarized virtual photon,

$$\frac{d\sigma}{d\Omega} = \sigma_0(1+\lambda\cos^2\theta), \qquad 3.$$

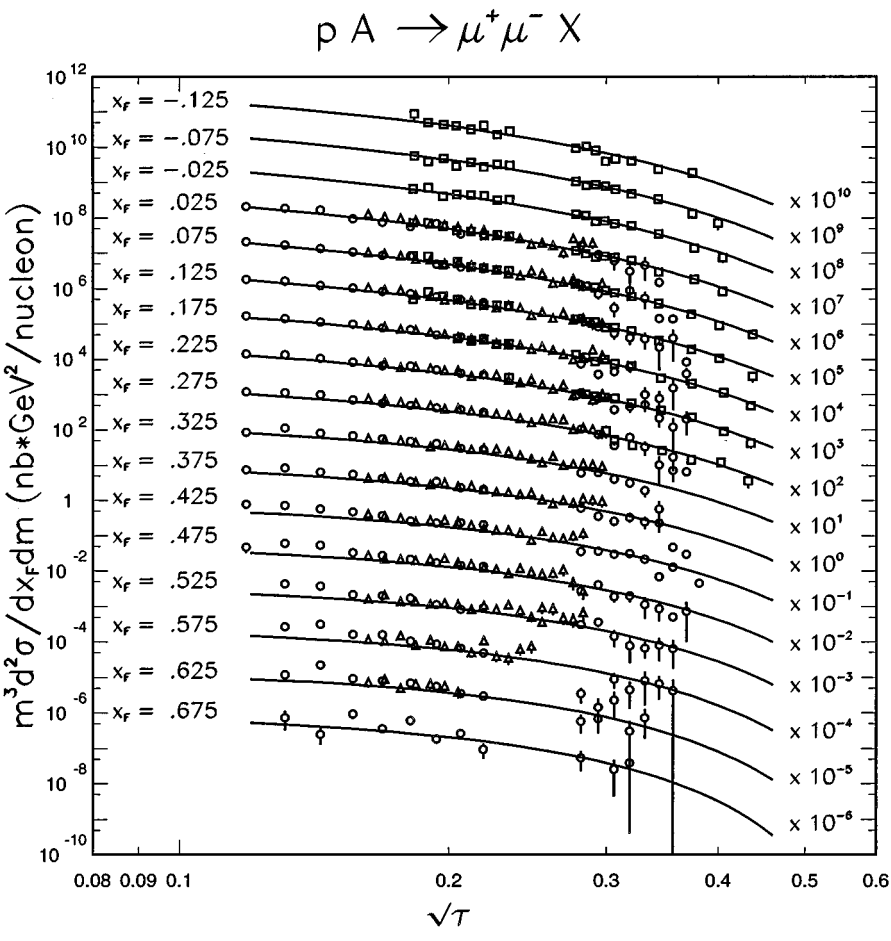

Figure 3 Proton-induced Drell-Yan production from experiments NA3 (8) (triangles) at 400 GeV/c, E605 (9) (squares) at 800 GeV/c, and E772 (10; PL McGaughey et al, unpublished data) (circles) at 800 GeV/c. The lines are absolute (no arbitrary normalization factor) next-to-leading order calculations for p + d collisions at 800 GeV/c using the CTEQ4M structure functions (11).

where θ is the polar angle of the lepton in the virtual photon rest frame and $\lambda = 1$. Early experimental data from both pion and proton beams (4) were consistent with this form but had large statistical errors.

Recently, E772 has performed a high-statistics study of the angular distribution for DY events (12) with masses above the Υ family of resonances. About 50,000 events were recorded from 800-GeV/c p + Cu collisions, using a copper beam dump as the target. Figure 4 shows the acceptance-corrected angular distribution, integrated over the kinematic variables. Analyzed in the Collins-Soper reference frame (13), the data yield $\lambda = 0.96 \pm 0.04 \pm 0.06$ (systematic).

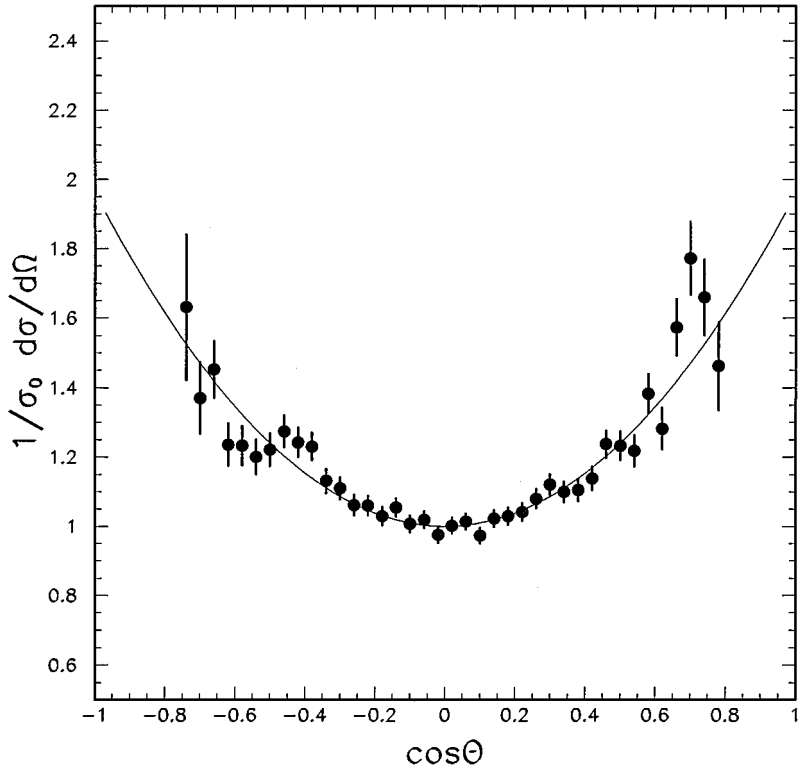

Figure 4 Drell-Yan angular distribution from Fermilab E772 (12): p + Cu collisions at 800 GeV/c. The dimuons cover the mass region $11 \leq M_{\mu^+\mu^-} \leq 17$ GeV/c^2 with $-0.3 \leq x_F \leq 0.8$ and $p_t \leq 6$ GeV/c. Mean values for p_t, x_F, and M are 1.4 GeV/c, 0.16, and 11.9 GeV/c^2, respectively. *Solid curve* is a fit to the data with the form $1 + \lambda \cos^2 \Theta$, where λ is $0.96 \pm 0.04 \pm 0.06$.

2.2 QCD and the Drell-Yan Process

Logarithmic scaling violation of the DY cross section is expected in leading order as for DIS. In the DY process, however, the virtual photon is timelike, $M^2 = Q^2 \geq 0$. Direct experimental confirmation has been difficult for the DY process [see the discussion in Freudenreich's review (7)] for two reasons. First, there is the complication that the cross section involves the convolution of two structure functions. Second, and more importantly, the DY process is experimentally well established as the major contribution to the dilepton spectrum only for $M \geq 4$ GeV/c^2. This is already a large value of Q^2 by DIS standards. Increasing M by a factor of five or so to provide enough lever arm to see the logarithmic change in $q(x, M^2)$ involves measurement of an exceedingly small cross section. Now that DY data have become an integral feature of global parton-structure fitting

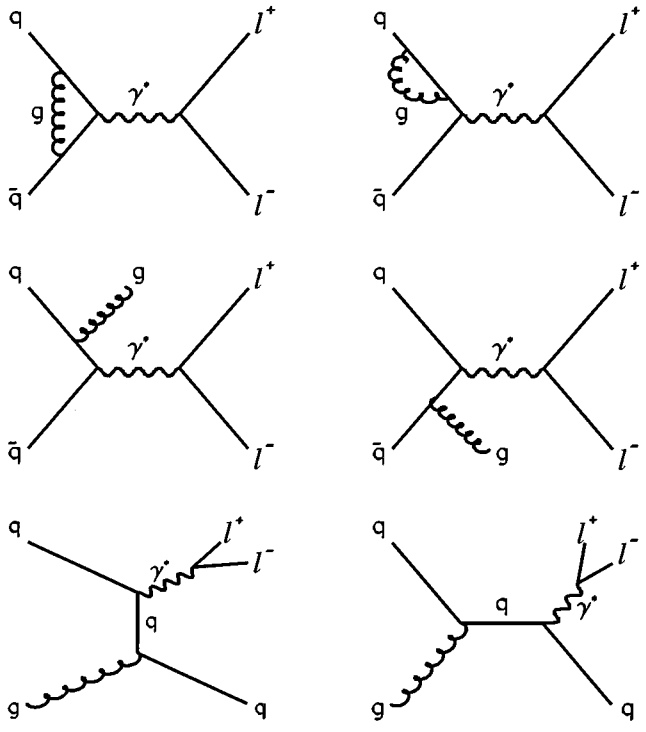

Figure 5 Feynman graphs for order α_s corrections to the Drell-Yan process.

programs, there is no longer much concern about testing the logarithmic scaling features of the data. An excellent summary of the use of DY data in structure function phenomenology appears in a recent review (14).

The importance of next-to-leading order (NLO; terms proportional to α_s) QCD corrections to the DY process has been well known since the mid-1980s (6, 15). Historically, two experimental features demanded theoretical improvement: first, the experimental cross section was about a factor of two larger than the parton-model value, and second, the distribution of dilepton transverse momenta extended to much larger values than are characteristic of the convolution of intrinsic parton momenta. Corrections to the DY mechanism at NLO largely fix these two problems. As shown in Figure 5, this comes at the expense of involving diagrams that seem to eliminate the simple parton interpretation of $q\bar{q}$ annihilation. Nevertheless, for most interpretations of the DY process, it is reasonably accurate to think in terms of parton-level $q\bar{q}$ annihilation with a modest increase in cross section.

QCD provides a procedure for calculating higher-order corrections to the DY process as well (16). In practice, NLO corrections are normally employed in QCD phenomenology. Figure 3 shows the typical agreement found when NLO calculations are compared—without normalization—to data.

Including higher-order QCD corrections to the DY process (17, 18) results in the more complicated form of the angular distribution,

$$\frac{d\sigma}{d\Omega} \propto 1 + \lambda \cos^2\theta + \mu \sin 2\theta \cos\phi + \frac{\nu}{2} \sin^2\theta \cos 2\phi, \qquad 4.$$

where ϕ is the azimuthal angle and λ, μ, and ν are angle-independent parameters. NLO calculations predict (19) small deviations from $1 + \cos^2\theta$ (<5%) for p_t below 3 GeV/c. The relevant scaling parameter for the magnitude of these deviations is p_t/Q, implying that NLO corrections become important when $p_t \simeq Q$. A relation, $1 - \lambda - 2\nu = 0$, developed by Lam & Tung (20), is analogous to the Callan-Gross relation in DIS. Measurements with pion beams at CERN (21) and at Fermilab (22) have shown that the Lam-Tung relation is clearly violated at large p_t.

Pion-induced DY experiments have unexpectedly shown that transverse photon polarization changes to longitudinal ($\lambda \simeq -1$) at large x_F (21–24). The x_F dependence of λ is qualitatively consistent with a higher-twist model originally proposed by Berger & Brodsky (25, 26). However, the quantitative agreement is poor. The model's basis can be described as follows. As x_F of the muon pair approaches unity, the Bjorken-x (momentum fraction) of the annihilating projectile parton must also be near unity. Thus, the whole pion contributes to the DY process. This can be treated with perturbation theory, with the result that the transverse polarization of the virtual photon becomes longitudinal. The angular distribution at large x_F becomes

$$\frac{d\sigma}{d\Omega} \propto (1-x)^2(1 + \lambda \cos^2\theta) + \alpha \sin^2\theta, \qquad 5.$$

where α is $\propto p_t^2/Q^2$.

Eskola et al (27) have shown that an improved treatment of the effects of nonasymptotic kinematics greatly improves quantitative agreement with the λ values from the pion data. Brandenburg et al (28) have extended the higher twist model to specifically include pion bound-state effects. They predict values for λ, μ, and ν that are in good agreement with the pion data at large x_F. Unfortunately, the results are quite sensitive to the choice of the pion Fock state wave functions, which are not well constrained by experimental data.

At this time, no comprehensive theory covering the full kinematic range of the experiments is available, nor is the observed violation of the Lam-Tung rule understood.

2.3 Factorization and Nuclear Size Effects

General discussions of factorization in the DY process and other QCD processes may be found in reviews by Collins & Soper (29) and Sterman et al (30).

A crucial requirement for the application of the DY process for the study of the quark structure of nuclei and nucleons (where most targets are actually nuclei) is that the factorized form of the cross section expressed by Equation 1 (or its QCD-corrected equivalent) remains valid for nuclei. Specifically, one wants assurance that $q_a(x, M^2)$ is the same for a proton that has traversed the diameter of

an atomic nucleus as it is for a free proton. Fortunately, this problem was analyzed extensively in the 1980s, particularly for the DY process (31–33). Within limits given approximately by

$$Q^2 \geq x_2 m_N L_A \langle l_\perp^2 \rangle, \qquad 6.$$

for hadron-nucleus collisions, initial-state interaction effects can be ignored for observables integrated over dilepton transverse momenta. In Equation 6, x_2 is the parton momentum fraction for a nucleus of mass A, m_N is the nucleon mass, and $l_\perp \approx 0.3$ GeV/c is the average momentum exchange in a quark-nucleon collision. With a path length $L_A = 2R_0A^{1/3}$, Equation 6 becomes $Q^2 \geq x_2 A^{1/3}$ GeV^2/c^2, a condition readily met for all nuclei. New nuclear dependence measurements, discussed in Sections 3.5–3.7, provide quantitative evidence of the absence of substantial initial-state interaction effects.

2.4 Experimental Detection of Continuum Lepton Pairs

The DY process was anticipated theoretically in 1970 (1). However, quantitative experiments had to wait until the late 1970s for the development of techniques permitting the measurement of picobarn cross sections in the presence of background processes many orders of magnitude larger. The most successful high-luminosity DY experiments have exploited inclusive dimuon detection in magnetic spectrometers whose apertures are filled with hadron absorbers. Hadron absorption near the target also reduces the backgrounds of muons from pion and kaon decays. Freudenreich's 1990 review (7) of lepton-pair production includes detailed descriptions of spectrometers built and operated during the 1970s and early 1980s. During the late 1980s and 1990s, two dimuon spectrometers remained operational at Fermilab and two at the CERN SPS. This review concentrates on data from these instruments. (The HELIOS collaboration at the SPS focused on the mass region below the J/ψ; hence, their work is not covered by this review.)

At Fermilab, a series of three experiments—E772, E789, and E866—used differing configurations of the large spectrometer located on a direct 800-GeV/c proton beam line in the Meson-East experimental area. The spectrometer (Figure 6) was originally constructed for E605, which studied dimuon production for $M_{\mu^+\mu^-} \geq 7$ GeV/c^2. The first two dipole magnets focus high-mass pairs into the spectrometer acceptance, thus avoiding the beam dump contained in the second magnet. The dump absorbs not only the beam but also the enormous flux of low-p_t secondaries from the target. The third large analyzing magnet provides a p_t kick of about 1 GeV/c for momentum analysis by the tracking system. The spectrometer is capable of operating at luminosities in the range 10^{35} cm^{-2} sec^{-1} with 10% interaction length targets and detection acceptances of ∼1–2% for the DY process. E772, E789, and E866 also exploited the copper beam dump as a second target (12, 34). The beam dump "target" has the advantage of a more open acceptance, permitting the measurement of angular distributions of muon pairs over a wide range of decay angles.

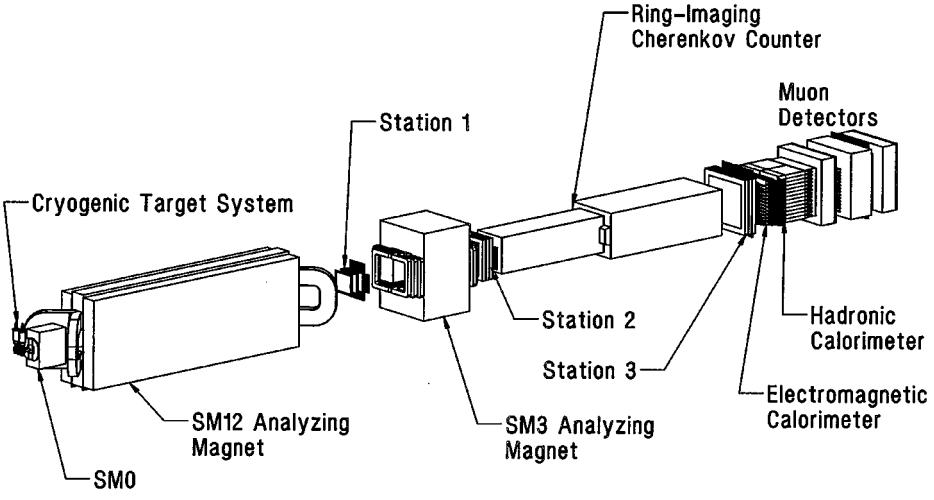

Figure 6 Schematic layout of the Meson-East focusing spectrometer at Fermilab.

The E705 collaboration at Fermilab operated an open-aperture (no hadron absorber) spectrometer that contributed important data to the study of the J/ψ and ψ' resonances and their decays (35).

The muon-pair spectrometer operated most recently at CERN was built originally for experiment NA10 (36). It consists of a large air-core toroid magnet with tracking chambers following the hadron absorber. In recent years, with substantial changes in its configuration, it has made unique contributions to the study of J/ψ production in relativistic heavy-ion collisions at the SPS (70), as well as to the determination of the $\bar{d}/\bar{u}$ asymmetry of the proton (38).

2.5 Backgrounds in Inclusive Dimuon Experiments

The E866 spectrum (Figure 1) illustrates the typical experimentally "safe" regions for DY muon pairs in fixed-target experiments with beams in the few-hundred GeV/c range. Below the J/ψ, a number of potential backgrounds, including the semileptonic decay of charmed hadrons, make the interpretation of the continuum more complex. Additionally, depending on details of the target and absorber configuration, pion and kaon decays can affect the low-mass spectrum. The data can be corrected for the latter contribution via subtraction of properly normalized like-sign muon pairs. But charm-pair decay, where this technique does not work, presents a more serious problem and ultimately limits the kinematic region that can be exploited. Ideally, the charm-pair decay contribution could be separated by use of a microvertex detector. To date, however, such a detector has not been combined with closed-aperture dimuon detection. The most systematic study of the contribution of charm production to the dimuon spectrum has been performed recently by the NA50 collaboration (37) in connection with measurements of J/ψ suppression in heavy-ion collisions. In NA50, the charm-pair decay continuum is

evaluated with the help of simulations of all contributing processes in the mass region just below the J/ψ.

3. DRELL-YAN PROCESS AND PARTON DISTRIBUTIONS

3.1 $\bar{d}/\bar{u}(x)$ Asymmetry of the Proton

From neutrino-induced DIS experiments, it is known that the strange-quark sea in the nucleon is roughly a factor of two less than the up- or down-quark sea (39). The lack of SU(3) flavor symmetry in the nucleon sea has been attributed to the much heavier mass of the strange quark. Until recently, it had been assumed that the distributions of $\bar{u}$ and $\bar{d}$ quarks were identical. Although the equality of $\bar{u}$ and $\bar{d}$ in the proton is not required by any known symmetry, it is a plausible assumption for sea quarks generated by gluon splitting. Because the masses of the up and down quarks are small compared with the confinement scale, nearly equal numbers of up and down sea quarks should result.

The assumption of $\bar{u}(x) = \bar{d}(x)$ can be tested by measurements of the Gottfried integral (40), defined as

$$I_G = \int_0^1 \left[F_2^p(x, Q^2) - F_2^n(x, Q^2)\right]/x\, dx = \frac{1}{3} + \frac{2}{3}\int_0^1 [\bar{u}_p(x) - \bar{d}_p(x)]dx, \qquad 7.$$

where F_2^p and F_2^n are the proton and neutron structure functions measured in DIS experiments. The second step in Equation 7 follows from the assumption of nucleon charge symmetry (Section 3.3). Under the assumption of a symmetric sea ($\bar{u} = \bar{d}$) the Gottfried Sum Rule (GSR) (40), $I_G = 1/3$, is obtained. Several early attempts (41–43) to test the GSR were inconclusive because the measurements did not reach small enough x, where large contributions to the integral are expected. Nevertheless, Field & Feynman (44) interpreted the early SLAC data (41), which gave $I_G(0.02 \rightarrow 0.8) = 0.20 \pm 0.04$, as an indication that the GSR is violated with $\bar{d}(x) > \bar{u}(x)$. They suggested that the Pauli-blocking effect suppressed $g \rightarrow u\bar{u}$ relative to $g \rightarrow d\bar{d}$, since protons contain two u-valence quarks and only one d-valence quark.

The most accurate test of the GSR was reported in 1991 by the New Muon Collaboration (NMC) (45), which measured F_2^p and F_2^n over the region $0.004 \leq x \leq 0.8$. They determined the Gottfried integral to be 0.235 ± 0.026, significantly below 1/3. This surprising result has generated much interest.

Although the violation of the GSR can be explained by assuming unusual behavior of the parton distributions at very small x (46), a more natural explanation is to abandon the assumption $\bar{u} = \bar{d}$. Specifically, the NMC result implies

$$\int_0^1 [\bar{d}(x) - \bar{u}(x)]\, dx = 0.148 \pm 0.039. \qquad 8.$$

We emphasize that only the integral of $\bar{d} - \bar{u}$ was deduced from the DIS measurements. The x dependence of $\bar{d} - \bar{u}$ remained unspecified.

The proton-induced DY process provides an independent means to probe the flavor asymmetry of the nucleon sea (47). An important advantage of the DY process is that the x dependence of $\bar{d}/\bar{u}$ can be determined. It is interesting to note that, as early as 1981, Fermilab E288 (48) reported evidence for a $\bar{d}/\bar{u}$ asymmetry, based on a measurement of the $p + d$ DY cross section. However, this interpretation depended sensitively on assumptions about the shape of the valence quark distributions and was not conclusive. Later, the Fermilab E772 collaboration (49) compared the DY yields from isoscalar targets with that from a neutron-rich (tungsten) target, and constraints on the nonequality of $\bar{u}$ and $\bar{d}$ in the range $0.04 \leq x \leq 0.27$ were set. More recently, the CERN experiment NA51 (38) carried out a comparison of the DY muon pair yield from hydrogen and deuterium using a 450 GeV/c proton beam. They found that $\bar{u}/\bar{d} = 0.51 \pm 0.04 \pm 0.05$ at $\langle x \rangle = 0.18$, a surprisingly large difference between the $\bar{u}$ and $\bar{d}$.

A DY experiment (E866), aiming at higher statistical accuracy and wider kinematic coverage than NA51, was recently completed (2) at Fermilab. This experiment also measured the DY muon pairs from 800-GeV/c protons interacting with liquid deuterium and hydrogen targets. The acceptance of the spectrometer was largest for $x_F = x_1 - x_2 > 0$. In this kinematic regime, the DY cross section is dominated by the annihilation of a beam quark with a target antiquark. The DY cross section ratio at large x_F is approximately given as

$$\frac{\sigma_{DY}(p+d)}{2\sigma_{DY}(p+p)} \approx \frac{1}{2}\left(1 + \frac{\bar{d}(x_2)}{\bar{u}(x_2)}\right). \qquad 9.$$

The ratio is unity when $\bar{d} = \bar{u}$. Figure 7 shows that the E866 measurement of this ratio clearly exceeds unity for an appreciable range in x_2.

Using an iterative procedure (2), values for $\bar{d}/\bar{u}$ were extracted by the E866 collaboration at $Q^2 = 54$ GeV^2/c^2. These are shown in Figure 8 along with the NA51 measurement. For $x < 0.15$, $\bar{d}/\bar{u}$ increases linearly with x and is in good agreement with the CTEQ4M (11) and MRS(R2) (50) parameterizations. However, a distinct feature of the data, not seen in either parameterization, is the rapid decrease toward unity of $\bar{d}/\bar{u}$ beyond $x = 0.2$.

The $\bar{d}/\bar{u}$ ratio, along with the CTEQ4M values for $\bar{d} + \bar{u}$, was used to obtain $\bar{d} - \bar{u}$ over the region $0.02 < x < 0.345$ (Figure 9). Being a flavor nonsinglet quantity, $\bar{d}(x) - \bar{u}(x)$ is decoupled from gluon splitting. From the results shown in Figure 9, one can obtain an independent determination (51) of the integral of Equation 8. E866 finds $0.100 \pm 0.007 \pm 0.017$, consistent with but roughly 2/3 of the value deduced by NMC.

Very recently, the HERMES Collaboration reported a semi-inclusive DIS measurement of charged pions from hydrogen and deuterium targets (52). Based on the differences between charged-pion yields from the two targets, the ratio $(\bar{d} - \bar{u})/(u - d)$ is determined in the kinematic range, $0.02 < x < 0.3$ and 1 GeV^2/c^2 $< Q^2 <$ 10 GeV^2/c^2. The HERMES results for $\bar{d} - \bar{u}$, shown in Figure 9, are consistent with the E866 results obtained at significantly higher Q^2.

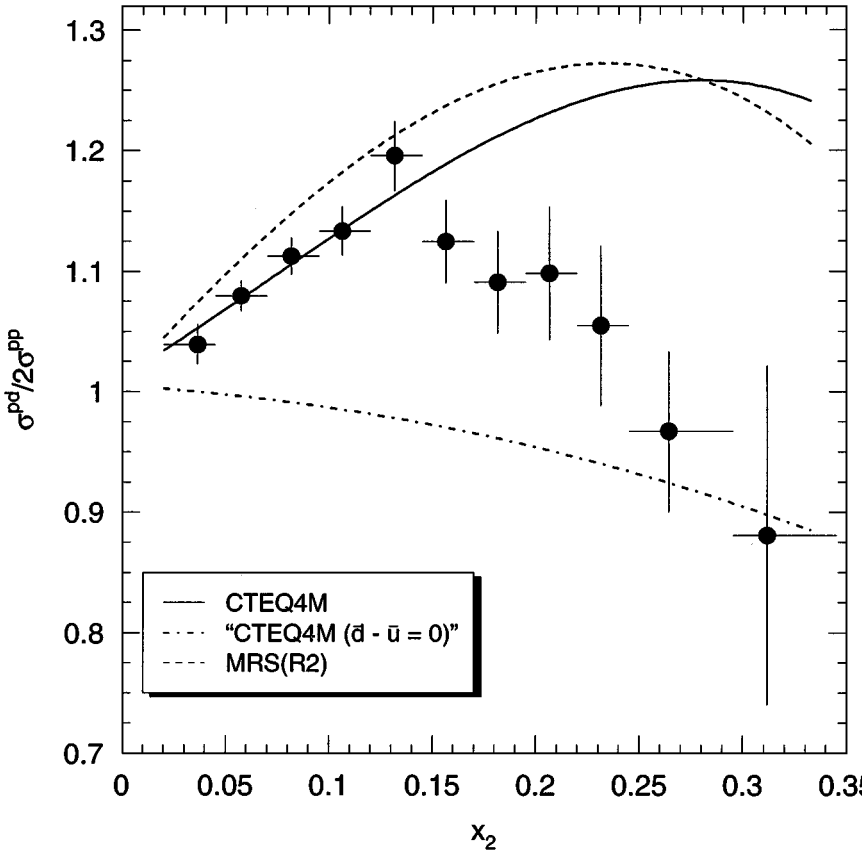

Figure 7 The ratio $\sigma^{pd}/2\sigma^{pp}$ of Drell-Yan cross sections vs x_2 from Fermilab E866 (2). The curves are next-to-leading order calculations, weighted by acceptance, of the Drell-Yan cross section ratio using the CTEQ4M (11) and MRS(R2) (50) parton distributions. In the lower CTEQ4M curve, $\bar{d} - \bar{u}$ was set to 0 to simulate a symmetric sea.

The E866 data clearly affect the current parameterization of the nucleon sea. The most recent structure functions of Martin et al (53) (MRST) included the E866 data in their global fit and produce results that are very different from the previous MRS(R2) parameterization (Figure 8). What is not so obvious is that the E866 data also affect the parameterization of the valence-quark distributions. Figure 10 shows the NMC data for $F_2^p - F_2^n$ at $Q^2 = 4$ GeV^2/c^2, along with the fits of MRS(R2) and MRST. It is instructive to decompose $F_2^p(x) - F_2^n(x)$ into contributions from valence and sea quarks:

$$F_2^p(x) - F_2^n(x) = \frac{1}{3}x\,[u_v(x) - d_v(x)] + \frac{2}{3}x[\bar{u}(x) - \bar{d}(x)]. \qquad 10.$$

As shown in Figure 10, the E866 data provide a direct determination of the sea-quark contribution to $F_2^p - F_2^n$. In order to preserve the fit to $F_2^p - F_2^n$, the MRST

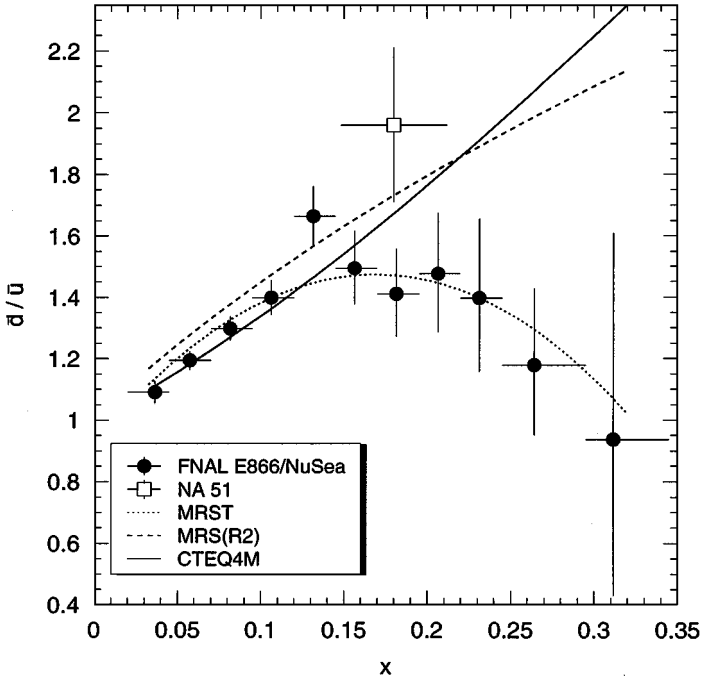

Figure 8 The ratio of $\bar{d}/\bar{u}$ in the proton as a function of x extracted from the Fermilab E866 (2) cross section ratio. The curves are from various parton distributions. Also shown is the result from NA51 (38) (open box).

parameterization of $u_v - d_v$ is significantly different from that of MRS(R2). Neither set reproduces $F_2^p - F_2^n$ in the range $x = 0.2$–0.3.

We now turn to the origin of the $\bar{d}/\bar{u}$ asymmetry (51, 54). As early as 1983, Thomas (55) pointed out that the virtual pions that dress the proton will lead to an enhancement of $\bar{d}$ relative to $\bar{u}$ via the (nonperturbative) "Sullivan process." Sullivan (56) previously showed that in DIS virtual mesons scale in the Bjorken limit and contribute to the nucleon structure function. Following the publication of the NMC result, many papers (57–65) treated virtual mesons as the origin of the $\bar{d}/\bar{u}$ asymmetry (see 54 for a recent review). Here the $\pi^+(\bar{d}u)$ cloud, dominant in the process $p \to \pi^+ n$, leads to an excess of $\bar{d}$ sea.

A different approach for including the effects of virtual mesons has been presented by Eichten et al (63) and further investigated by other authors (64, 65). In chiral perturbation theory, the relevant degrees of freedom are constituent quarks, gluons, and Goldstone bosons. In this model, a portion of the sea comes from the couplings of Goldstone bosons to the constituent quarks, such as $u \to d\pi^+$ and $d \to u\pi^-$. The excess of $\bar{d}$ over $\bar{u}$ is then simply due to the additional valence u quark in the proton.

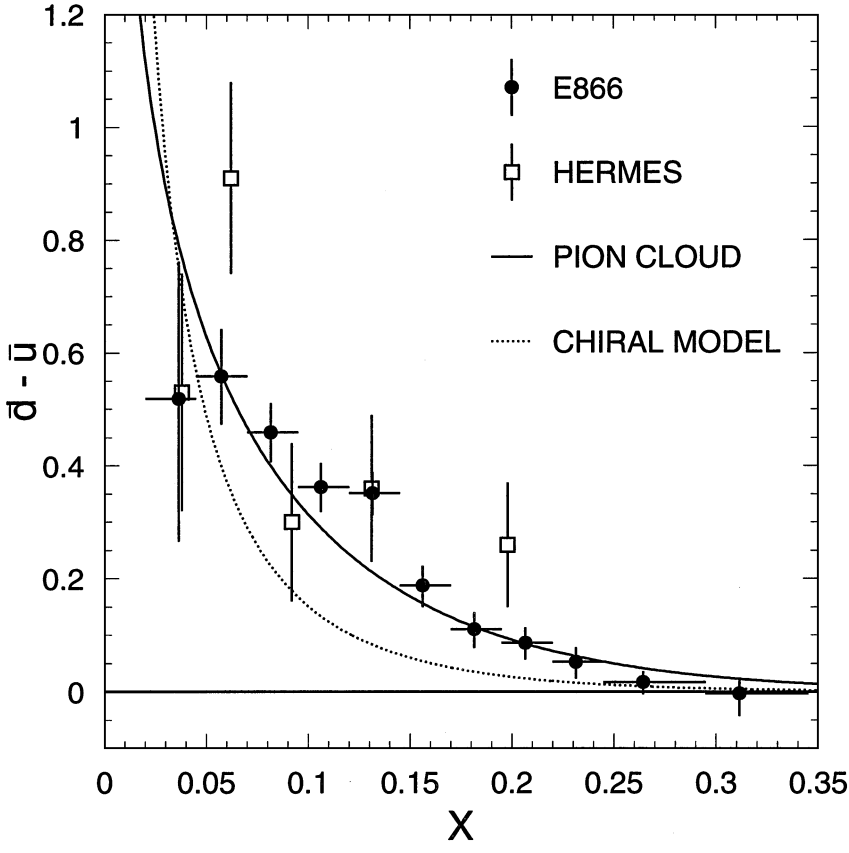

Figure 9 Comparison of the E866 (2) $\bar{d} - \bar{u}$ results at $Q^2 = 54$ GeV^2/c^2 with the predictions of pion-cloud and chiral models as described in the text. The data from HERMES (52) are also shown.

The x dependences of $\bar{d} - \bar{u}$ and $\bar{d}/\bar{u}$ obtained by E866 provide important constraints for theoretical models. Figure 9 compares $\bar{d}(x) - \bar{u}(x)$ from E866 with a virtual-pion model calculation, following the procedure detailed by Kumano (58). A dipole form factor was used, with cutoff parameters $\Lambda = 1.0$ GeV (0.8 GeV) for the πNN ($\pi N\Delta$) vertex. Λ is the cutoff parameter for the pion form factor. Figure 9 (dotted curve) also shows the predicted $\bar{d} - \bar{u}$ from the chiral model. We follow the formulation of Szczurek et al (65) to calculate $\bar{d}(x) - \bar{u}(x)$ at $Q^2 = 0.25$ GeV^2/c^2 and then evolve the results to $Q^2 = 54$ GeV^2/c^2. The chiral model places more strength at low x than does the virtual-pion model. This difference reflects the fact that the pions are softer in the chiral model, since they are coupled to constituent quarks that carry only a fraction of the nucleon momentum. The x dependence of the E866 data favors the virtual-pion model over the chiral

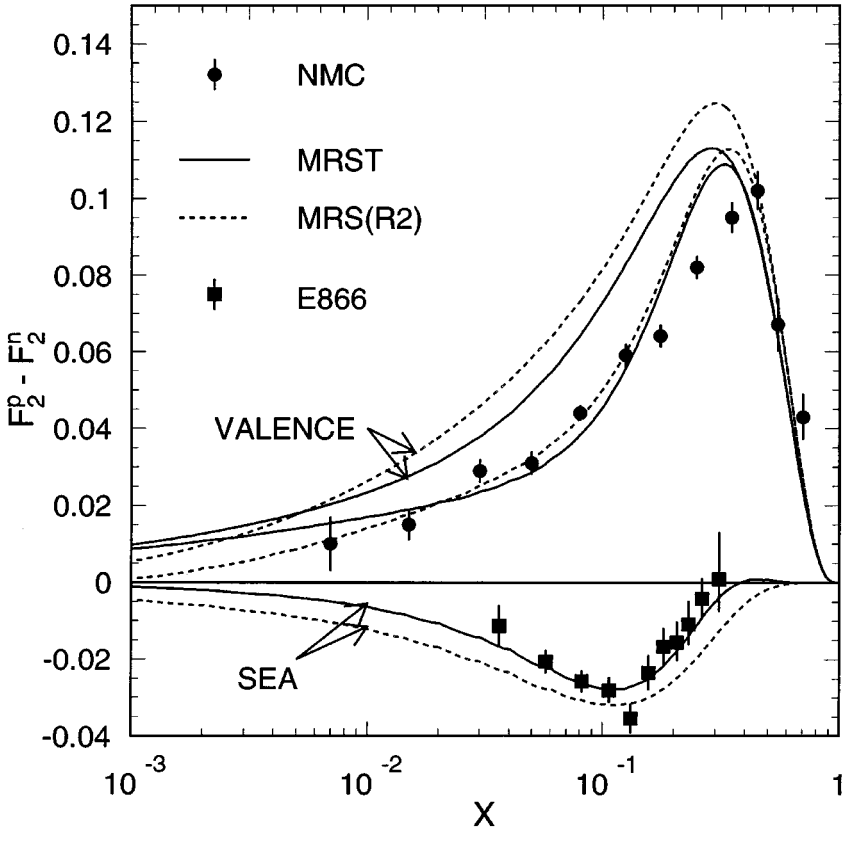

Figure 10 $F_2^p - F_2^n$ as measured by NMC (45) at $Q^2 = 4$ GeV^2/c^2 compared with predictions based on the MRS(R2) (50) and MRST (53) parameterizations. Also shown are the E866 results (2), evolved to $Q^2 = 4$ GeV^2/c^2, for the sea-quark contribution to $F_2^p - F_2^n$. For each prediction, the top (bottom) curve is the valence (sea) contribution and the middle curve is the sum of the two.

model, suggesting that correlations between the chiral constituents should be taken into account.

The chiral and the meson-cloud models both predict that the $\bar{u}$ and $\bar{d}$ quarks will carry negligible amount of the proton's spin (51, 63, 66), a prediction that remains to be tested. Another interesting consequence of the meson-cloud model is that the s and $\bar{s}$ distributions in the proton could have very different shapes, even though the net amount of strangeness in the proton vanishes (67, 68). By comparing the ν and $\bar{\nu}$ induced charm production, the CCFR collaboration found that the s and $\bar{s}$ distributions are very similar (69). Dimuon production experiments using $K^{\pm}$ beams might provide an independent determination of the $s/\bar{s}$ ratio of the proton.

3.2 Polarized Drell-Yan and $W^{\pm}$ Production

The spin structure of the nucleon has been extensively investigated by polarized DIS (70, 71) during the past 10 years. Much of the excitement in this field has come from the finding that quarks contribute a surprisingly small fraction to the nucleon's total helicity. As a result, considerable interest has been centered on QCD processes in hadronic collisions, where polarized gluon and antiquark effects are directly manifested.

Polarized DY production and $W^{\pm}$ production have great potential for providing qualitatively new information about antiquark polarization.[2] Because polarized proton collisions will become feasible at the Relativistic Heavy Ion Collider (RHIC) facility starting in 2001, it is timely to review the type of information that such studies will provide.

The longitudinal spin asymmetry (requiring polarization of both protons) in the DY process is, in leading order, given by (72)

$$A_{LL}^{DY}(x_1, x_2) = \frac{\sum_a e_a^2[\Delta q_a(x_1)\Delta\bar{q}_a(x_2) + \Delta\bar{q}_a(x_1)\Delta q_a(x_2)]}{\sum_a e_a^2[q_a(x_1)\bar{q}_a(x_2) + \bar{q}_a(x_1)q_a(x_2)]}, \qquad 11.$$

with $\Delta q_a \equiv q_a^+ - q_a^-$. The superscripts refer to parton spin projections parallel (+) or antiparallel (−) to the proton's spin projection.[3] One can simplify this equation by choosing the kinematic region $x_F \geq 0.2$, where a single term, $u(x_1)\bar{u}(x_2)$, dominates the denominator of Equation 11 (see Section 3.1). The equation thus becomes

$$A_{LL}^{DY}(x_1, x_2) \approx A_{LL}^{pDIS}(x_1) \times \frac{\Delta\bar{u}}{\bar{u}}(x_2), \qquad 12.$$

where the asymmetry measured in DIS on polarized protons is $A_{LL}^{pDIS}(x) = g_1(x)/F_1(x)$. Thus, the helicity asymmetry in polarized p-p collisions is a measure of the antiquark polarization at x_2 in one proton, with the other proton providing a quark at x_1 with known polarization (72, 73). [This derivation also requires that the DIS structure function, $g_1^n(x)$, be approximately zero, a condition well met for $x \geq 0.2$.]

A closely related reaction, the production of $W^{\pm}$, has been analyzed theoretically (77). The parity-violating nature of $W^{\pm}$ production leads to some essential differences. First, only one of the two beams needs to be polarized. Second, $W^{\pm}$ leptonic decay produces a charged lepton, which can be detected, and a neutrino, which cannot. Thus, the measurement necessarily integrates over some range of

[2]Quarkonium production has also been considered as a means of determining gluon polarization. However, unresolved issues about the mechanism of quarkonium production (see Section 4) prevent its application as even a qualitative measure of ΔG, at least in the early stages of polarized hadronic collisions.

[3]Next-to-leading-order QCD corrections to Equation 11 have been evaluated by several authors (74–76). They are generally small in most of the DY kinematic range.

x_1 and x_2. Using the kinematics treated previously for DY production, one finds, for Ws produced at negative x_F [opposite to the direction of the polarized beam (x_1)],

$$A_L^{W^+} \approx -\frac{\Delta \bar{d}}{d}(x_2), \quad \text{and} \quad A_L^{W^-} \approx -\frac{\Delta \bar{u}}{\bar{u}}(x_2). \qquad 13.$$

This is similar to Equation 12 but without the quark polarization factor multiplying the antiquark asymmetry. For Ws produced at positive x_F, one finds

$$A_L^{W^+} \approx \frac{\Delta u}{u}(x_2), \quad \text{and} \quad A_L^{W^-} \approx \frac{\Delta d}{d}(x_2). \qquad 14.$$

In the DY process (or in Z^0 production, but not $W^{\pm}$ production), it is also possible to measure a new structure function, called transversity, which is a correlation between quark momentum and its perpendicular spin component (78). The transversity is not measurable in inclusive DIS (79). It is measurable, in principle, in collisions of polarized protons whose spins are aligned perpendicular to the plane of dilepton detection. A nonzero transverse spin correlation in the DY process would clearly require both quark and antiquark transversities to be nonzero. A theoretically ideal, but currently impossible, experiment would be the measurement of the transverse spin correlation and hence the quark transversity of the proton via polarized $p\bar{p}$ collisions.[4]

Studies of both continuum DY and $W^{\pm}$ production in polarized p-p collisions are planned at RHIC (80). The scaling properties of the DY cross section,

$$d^2\sigma/d\sqrt{\tau}dx_F \propto 1/s, \qquad 15.$$

combined with the kinematic relation, Equation 2, greatly favor the lowest beam energy consistent with the production of DY pairs in the "safe" region. Thus, detection of muon pairs with $x_1 = 0.25$, $x_2 = 0.4$(M = 5 GeV/c^2) at $\sqrt{s} =$ 50 GeV has 16 times higher cross section than detection of 20-GeV/c^2 pairs at $\sqrt{s} = 200$ GeV. Because of its high threshold, $W^{\pm}$ is feasible only at the highest proton energy of RHIC, $\sqrt{s} = 500$ GeV.

3.3 Charge Symmetry Violation in Parton Distributions

Charge symmetry is believed to be well respected in strong interaction. Extensive experimental searches for charge symmetry violation (CSV) effects in various nuclear processes reveal an amount on the order of 1% (81). This is consistent with the expectation that CSV effects are caused by electromagnetic interaction and the small mass difference between the u and d quarks (82).

It has been generally assumed that the parton distributions in hadrons obey charge symmetry. This assumption enables one to relate the parton distributions

[4]An estimate of the transversity asymmetry in the bag model (79) indicates that it peaks at large x, as does the helicity asymmetry. Polarized $p\bar{p}$ collisions at large x would thus yield a large experimental asymmetry.

in the proton and neutron in a simple fashion, $u_p(x) = d_n(x), d_p(x) = u_n(x)$, etc. Indeed, charge symmetry is usually assumed in the analysis of DIS and DY experiments, which often use nuclear targets containing both protons and neutrons. Charge symmetry is also implicit in the derivation of many QCD sum rules, including the Gottfried sum rule, the Adler sum rule, and the Bjorken sum rule.

The possibility that charge symmetry could be significantly violated at the parton level has been discussed recently by several authors (83–89). Ma and collaborators (83, 84) pointed out that the violation of the GSR can be caused by CSV as well as by flavor asymmetry of the nucleon sea. They also showed that DY experiments, such as NA51 and E866, are subject to both flavor asymmetry and CSV effects. Using the bag model, Rodionov et al (87) showed that a significant CSV effect of ~5% could exist for the "minority valence quarks" [i.e. $d_p(x)$ and $u_n(x)$] at large x ($x > 0.4$). A model study (89) of CSV for sea quarks shows that the effect is very small, roughly a factor of 10 less than for valence quarks. Londergan & Thomas have recently reviewed the role of CSV for parton distributions (90).

Evidence for a surprisingly large CSV effect was recently reported by Boros et al (91, 92) based on an analysis of F_2 structure functions determined from muon and neutrino DIS experiments. A large asymmetry, $\bar{d}_n(x) \sim 1.25\bar{u}_p(x)$ for $0.008 < x < 0.1$, is apparently needed to bring the muon and neutrino DIS data into agreement. How would this finding, if confirmed by further studies, affect the E866 analysis of the flavor asymmetry? First, CSV alone could not account for the E866 data. In fact, an even larger amount of flavor asymmetry is required to compensate for the possible CSV effect (92). Second, there has been no indication of CSV for $x > 0.1$. Thus, the large $\bar{d}/\bar{u}$ asymmetry from E866 for $x > 0.1$ is not affected.

3.4 Parton Distributions of Mesons and Hyperons

Dilepton production using meson or hyperon beams offers a means of determining parton distributions of these unstable hadrons. Many important features of nucleon parton distributions, such as the flavor structure and the nature of the nonperturbative sea, find their counterparts in mesons and hyperons. Information about meson and hyperon parton structure could provide valuable new insight into nucleon parton distributions. Furthermore, certain aspects of the nucleon structure, such as the strange quark content of the nucleon, could be probed with kaon beams.

Pion-induced DY cross sections have been measured in several high-statistics experiments (93–96). These data form the basis for a global analysis (97) to extract the pion structure functions. Although a large amount of DY data exists for π^- beams, the corresponding data for π^+ beams are surprisingly meager. The π^+ data are crucial for separating the valence and sea-quark distributions in pions. The lack of high-statistics π^+ DY data is responsible for our poor knowledge of the sea-quark distributions in pions. Future DY experiments using high-energy π^+ beams ($P_\pi > 400$ GeV/c) are required to study the sea of the pion.

The advent of the Fermilab Main Injector (FMI) opens the possibility of performing DY measurements with intense pion and kaon beams. The relatively low

beam momenta are suitable for studying parton distributions at large x. Londergan et al (86) suggested that a comparison between π^+ and π^- DY cross sections on hydrogen and deuterium targets could test the charge symmetry of the valence quark distributions in the nucleon.

Very few data exist for the kaon-induced DY process. The NA3 collaboration (98) obtained several hundred DY events with a K^- beam. By comparing the K^- with the π^- DY data, they found evidence that the $\bar{u}$ distribution in K^- is significantly softer than in the π^-. Because this effect is the largest at large x_1, the kaon beam at the FMI could be used for further studies.

No data exist for hyperon-induced dilepton production. The observation of a large $\bar{d}/\bar{u}$ asymmetry in the proton has motivated Alberg et al (99, 100) to consider the sea-quark distributions in the Σ. The meson-cloud model implies a $\bar{d}/\bar{u}$ asymmetry in the Σ^+ even larger than that of the proton. However, the opposite effect is expected from SU(3) symmetry. Although relatively intense Σ^+ beams have been produced for recent experiments at Fermilab, this experiment appears to be very challenging because of large pion, kaon, and proton contaminations in the beam.

3.5 Nuclear Dependence of the Drell-Yan Process

The famous nuclear dependence of DIS, referred to as the European Muon Collaboration (EMC) effect, was discovered in the early 1980s (101, 102). Figure 11 shows the general features of the EMC effect, with data from the NMC (103).

In 1986, the Fermilab E772 collaboration proposed to measure the nuclear dependence of the DY process as a means of further elucidating the EMC effect and the issue of parton structure in nuclei in general. It is clear from the dominance of the term $u(x_1)\bar{u}(x_2)$ in the kinematic region, $x_F \geq 0.2$, that the proton-induced DY process provides a view of the nucleon that is complementary to DIS. In the E772 configuration, typically more than 90% of the cross section arises from this term. In contrast, only about 15% of the cross section in DIS at $x \sim 0.1$ is due to antiquarks.

The results from E772 (104) (Figures 11 and 12) show that there is no enhancement of the antiquark distribution in nuclei. Even in the absence of a specific model calculation, the lack of an antiquark enhancement in nuclei seems at odds with the picture of nuclei as nucleons bound by the exchange of mesons. [Models of the EMC effect have been reviewed recently (102). We do not present a complete overview here.]

In order to be more quantitative, it is necessary to invoke a model calculation. The pion excess model, based on the convolution framework of Sullivan (56), is most specific in predicting the nuclear antiquark distribution. After many years of studying this issue (see e.g. 105), the conventional wisdom is that there are "excess" pions in nuclei, which are in part responsible for nuclear binding (106). In terms of the pion excess model, the E772 results set stringent limits on the collectivity of the πNN vertex inside nuclei. It appears that the nuclear pion field

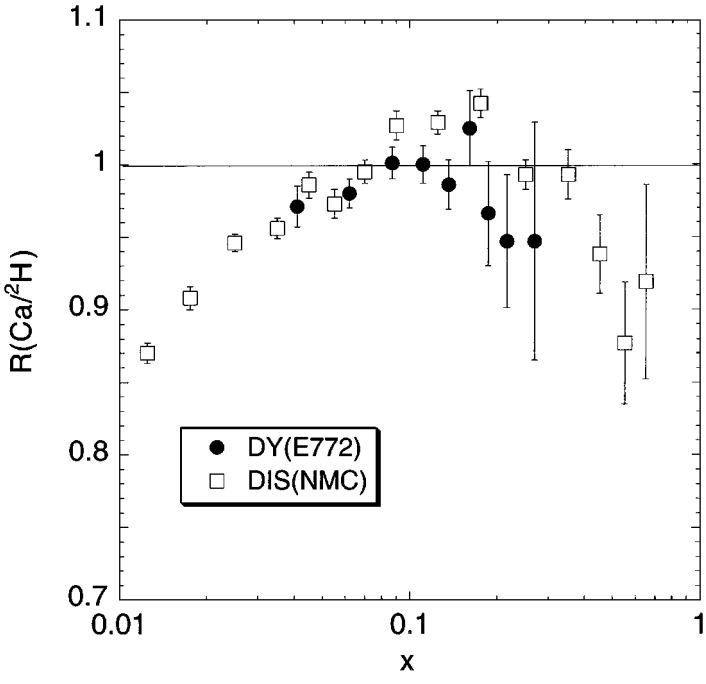

Figure 11 Comparison of the cross section per nucleon ratios $\sigma_{Ca}/\sigma_{^2H}$ for DY production (104) and DIS (103).

is not collective at all; there are no more pions surrounding the average nucleon in a heavy nucleus than there are in the weakly bound system, deuterium. This contradicts conventional wisdom and is also at odds with sophisticated new solutions of the nuclear many-body problem using realistic nuclear forces (106–109). When these techniques are applied at central nuclear-matter density, they predict a substantially increased pion density, $\Delta n_\pi = 0.18$ per nucleon (106, 108).[5]

Using the Sullivan model, Brown et al (110) propose a solution that appears to maintain much of the conventional understanding that nuclear binding results from meson exchange. They achieve agreement with the E772 antiquark ratio by postulating a decrease in the effective masses of hadrons inside nuclei resulting from a partial restoration of chiral symmetry. In view of the strong recent interest in chiral symmetry restoration in relativistic heavy-ion collisions, this is a fascinating explanation. However, it is far from being universally accepted as the answer to the mystery of antiquarks in nuclei. More recently, Koltun (111) has advanced another suggestion that may reconcile the absence of an antiquark enhancement with conventional nuclear theory.

[5]Reference 108 contains a correction to the pion excess per nucleon calculated originally in Reference 106.

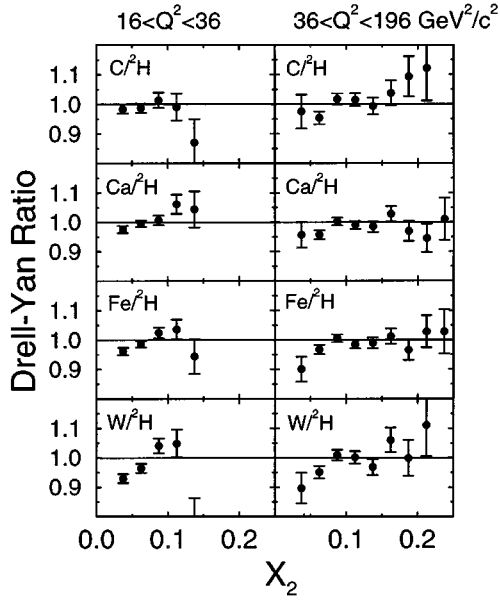

Figure 12 Ratio of Drell-Yan cross sections per nucleon for heavy nuclei to deuterium versus target momentum fraction from E772 (104). The two columns show data for different bins of $Q^2 = M^2$.

3.6 Shadowing

In the past decade, shadowing—the reduction of the cross section per nucleon for nuclear targets at small x—has been very well characterized experimentally in DIS (103). The experimental signature appears clearly in Figure 11, where the DIS ratio falls below unity for $x \leq 0.08$. Theoretically, shadowing has been studied extensively in the past 10 years (see 102 for many seminal references). A recent study by Kopeliovich et al (112) presents an alternative view to the parton recombination picture of Mueller & Qiu (113).

Shadowing is also expected in hadronic processes. However, the beam energies available at fixed-target facilities have limited investigations thus far. The reason is clear from the following numerical example. In order to have a large enough cross section, one needs $x_1 \leq 0.5$. This limit, combined with the requirement $M \geq 4$ GeV/c^2 at $\sqrt{s} = 38.9$ GeV (800 GeV/c fixed target) in Equation 2, yields $x_2 \geq 0.02$. Similar arguments apply to fixed-target inclusive direct photon production. To date, the only experimental evidence for shadowing in hadronic reactions is the reduction in the nuclear dependence seen in Figures 11 and 12 from E772 (104). The DY and DIS ratios for the same targets show similar behavior, although the x range is more limited for the DY data.

It has been suggested that the reduction in the DY nuclear dependence ratio at small x_2 is more appropriately ascribed to the effects of initial-state energy

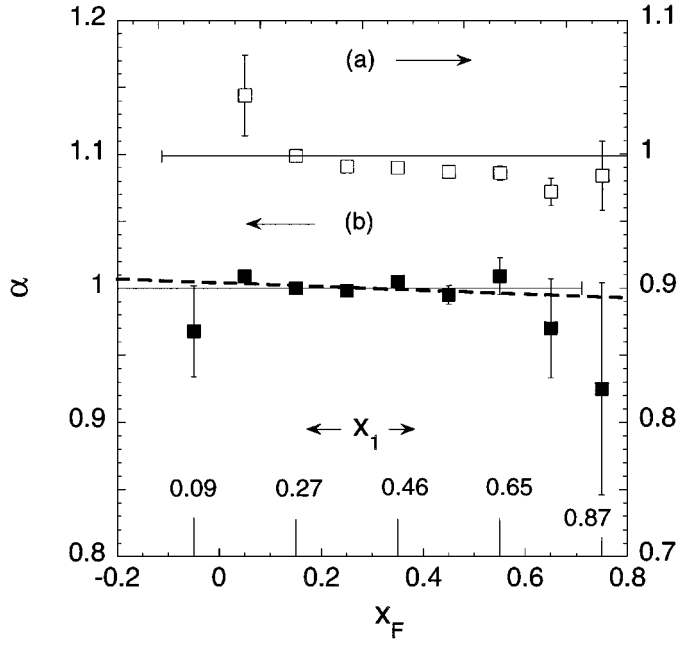

Figure 13 Nuclear dependence coefficient α for the Drell-Yan process (104) versus x_F for (*a*) $x_2 \leq 0.075$, right scale, and (*b*) $x_2 \geq 0.075$, left scale. Thin solid lines show $\alpha = 1$. The dashed line is a linear least-squares fit to the lower points. Also shown is the mean value of x_1 for (*b*).

loss (114, 115). This is unlikely in view of Figures 12 and 13 and the discussion in Section 3.7. Figure 12 shows the nuclear dependence ratios for two different ranges of Q^2 (M^2). It is clear that the reduction at small x_2 persists despite the significant change in the x_F range for the different Q^2 cuts. An alternative view is obtained by fitting all four target ratios in terms of the common parameter α, defined by $\sigma_A = \sigma_N \times A^\alpha$. A deviation of α from unity indicates a cross section that is not proportional to the number of target nucleons. Figure 13 shows α versus x_F for two bins of x_2, one in the shadowing region (upper) and one outside it (lower). The lower plot exhibits no statistically significant dependence on x_F or x_1, again showing that the suppression is correlated with the target momentum fraction.

Shadowing in the $p + A$ DY process is largely due to antiquarks in the nucleus, unlike in DIS, where quarks dominate for most of the explored region. Although shadowing effects are expected for antiquarks and gluons, there is no known requirement that they be identical (116) to those for quarks. Nevertheless, direct comparison of DY and DIS data for Ca versus ^{2}H (Figure 11) shows them to be identical within statistics. In contrast, in the region $0.1 \leq x \leq 0.2$, where DIS shows a modest enhancement in the ratio, no corresponding increase occurs in the

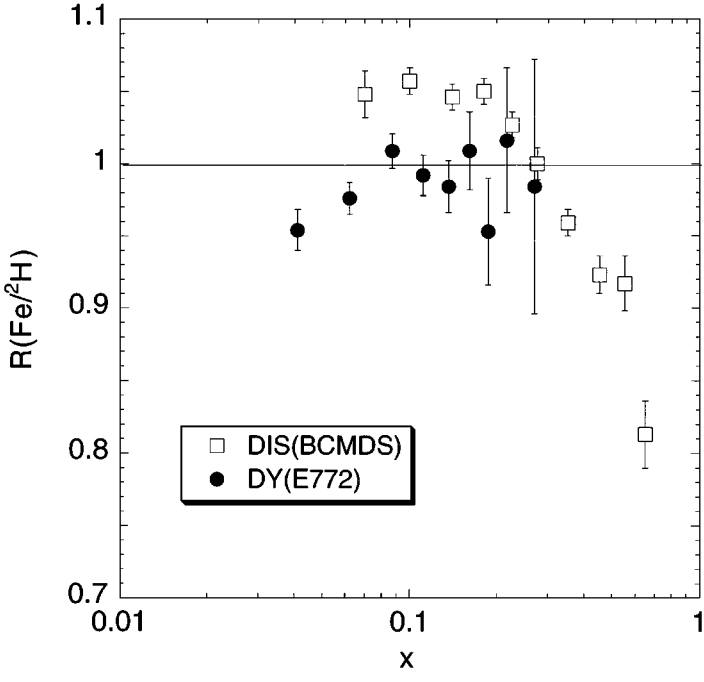

Figure 14 Comparison of the cross section per nucleon ratios $\sigma_{Fe}/\sigma_{^2H}$ for DY production (104) and DIS (117).

DY ratio. This is also evident in Figure 14, which compares Fe versus ^{2}H for DIS and the DY process.

3.7 Multiple Scattering and Energy Loss

The energy loss of fast partons moving through hadronic matter has received extensive theoretical attention (114, 118–121). Recently, Baier et al (121) have derived a connection between the longitudinal energy loss and the mean p_t accumulated in multiple parton-nucleon scatterings that is directly applicable to experiment. Specifically,

$$-dE/dz = \frac{1}{4}\alpha_s N_c p_t^2, \qquad 16.$$

where $N_c = 3$. The theory of Baier et al yields the nonintuitive result that the total energy loss is proportional to square of the path length traversed.

The nuclear dependence of the DY process offers a particularly clean way to test this relationship, since multiple scatterings are confined to the initial-state quark's traversal of nuclear matter. CERN experiment NA10 (122) made the first measurements of the nuclear dependence of the DY process as function of p_t. The ratio

TABLE 1 Values of $\Delta\langle p_t^2\rangle \equiv \langle p_t^2\rangle(A) - \langle p_t^2\rangle(^2H)$ for the DY process. For NA10, the mass range for muon pairs was, respectively, $M \geq 4.35$ GeV/c^2 at 140 GeV/c and $M \geq 4.2$ GeV/c^2 at 286 GeV/c. The mass range of the Υ(8.5 GeV/c$^2 < M < 11$ GeV/c^2) was also excluded. For E772, the range was $M \geq 4$ GeV/c^2, with the exclusion of 9 GeV/c$^2 \leq M \leq 11$ GeV/c^2

Experiment	Beam	A	$\Delta\langle p_t^2\rangle$(GeV^2/c^2)
NA10 (122)	140 GeV/c π^-	W	$0.16 \pm 0.03 \pm 0.03$ (syst.)
	286 GeV/c π^-	W	$0.15 \pm 0.03 \pm 0.03$ (syst.)
E772 (123)	800 GeV/c p	C	$-0.011 \pm 0.015 \pm 0.03$ (syst.)
		Ca	$0.046 \pm 0.012 \pm 0.03$ (syst.)
		Fe	$0.053 \pm 0.012 \pm 0.03$ (syst.)
		W	$0.106 \pm 0.016 \pm 0.03$ (syst.)

σ_A/σ_N was found to increase with increasing p_t. E772 (123) extended the nuclear dependence measurements by determining $\Delta\langle p_t^2\rangle$, where $\Delta\langle p_t^2\rangle \equiv \langle p_t^2\rangle(A) - \langle p_t^2\rangle(^2H)$, for DY production for a series of nuclei. Table 1 lists $\Delta\langle p_t^2\rangle$ from NA10 and E772. The E772 values (PL McGaughey, JM Moss, JC Peng, unpublished data) have changed slightly[6] from those given in Reference 123. Figure 15 shows a fit to the E772 data with a nuclear dependence of the form $\langle p_t^2\rangle(A) \propto A^{1/3}$.

To convert $\Delta\langle p_t^2\rangle$ to an energy loss, one can approximate a nucleus by a uniform sphere of radius $R_0 A^{1/3}$. This yields a mean path length of $\frac{3}{4} R_0 A^{1/3}$ for the initial-state partons. Then, using Equation 16, one finds $\Delta E \approx 0.59$ GeV for the tungsten data from E772. In the lab frame, $\delta x_1 \approx \Delta E / E_{beam} = 7.4 \times 10^{-4}$, an exceedingly small nuclear effect versus x_1 or x_F. The dashed line in Figure 13 (lower plot) is a linear fit to the data. This slope can be converted into an initial-state energy loss by using the shape of the accepted spectrum versus x_1. This yields $\Delta E = 2.0 \pm 1.7$ GeV, which is consistent with, but weaker than, the limit determined from the p_t broadening.

The absence of a sizable quark energy loss is in qualitative accord with the finding of a weak nuclear dependence for the production of leading hadrons in DIS (124, 125). As has been noted before (121), however, an interpretation of the nuclear dependence of the p_t broadening in photon-induced dijet production (126) via Equation 16 leads to a very large energy-loss effect. We have no new insight into this dilemma. However, it is clear that further experimental tests of Equation 16 are needed. Understanding how fast partons propagate through hadronic matter is crucial for understanding highly relativistic heavy-ion collisions and the possible production of the QGP.

[6]The new evaluation is based on an analysis of $d\sigma/dp_t^2$ for ^2H(10), not available previously.

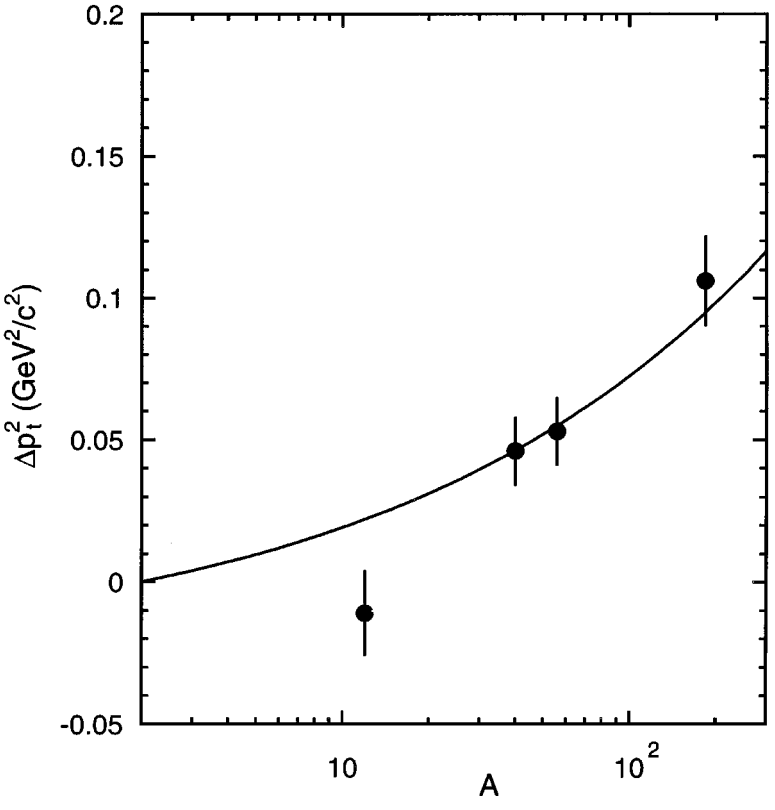

Figure 15 $\Delta\langle p_t^2\rangle \equiv \langle p_t^2\rangle(A) - \langle p_t^2\rangle(^2H)$ versus A for the DY process from E772 (123; PL McGaughey, JM Moss, JC Peng, unpublished data). Solid curve corresponds to $0.027((A/2)^{1/3} - 1)$.

4. QUARKONIUM PRODUCTION

4.1 Quarkonium Production in Hadronic Collisions

Much of this section focuses on aspects of the nuclear dependence of quarkonium production. However, it is important to appreciate the impact of the experimental results from the Tevatron Collider on the theory of quarkonium production in hadronic collisions. Braaten et al (3) have recently reviewed this subject.

In 1995, the CDF collaboration published cross sections (127) for vertex-identified (i.e. not arising from b-quark decay) J/ψ and ψ' production at very large p_t—a particularly advantageous region for comparison with theory. The result was that the time-honored color-singlet production model underpredicted the cross section by factors as large as 30. Motivated by this spectacular failure, intense theoretical activity has focused on more general production mechanisms, including

color-octet channels. Color-octet production has become the new paradigm in theoretical descriptions of quarkonium production.

At fixed-target energies, however, the production of quarkonia at relatively low p_t presents a challenge to the new models (128–130). The effects of color-octet channels are reduced, and there are still problems in accounting for the observed small polarization. It is clear that the continuing theoretical debate about mechanisms of quarkonium production will influence, and be influenced by, the large nuclear dependence effects discussed below.

4.2 Nuclear Dependence of Quarkonium Production

In contrast to the DY process, large nuclear effects are found in the hadronic production of the J/ψ resonance (131–134). Whether induced by protons, antiprotons, or pions over a wide range of beam energies, there is a significant reduction in the cross section per nucleon for heavy nuclei.[7]

Using 800-GeV/c protons, E772 (137) was able to resolve the J/ψ and ψ' resonances for the first time in a nuclear-dependence measurement. Surprisingly, the E772 collaboration found that the nuclear dependences for the two states were identical within statistics. Equally unexpected, they found a significant nuclear dependence in the yields of the Υ, Υ', and Υ'' resonances (123), although less than that observed for the J/ψ and ψ'. Again, within worse statistics, the nuclear dependences of the Υ and the combined Υ' and Υ'' were the same. Figure 16 summarizes the integrated nuclear-dependence data from E772.

CERN experiment NA38 (138) has confirmed the observation of equal nuclear suppression of J/ψ and ψ' states in p + A collision at 200 GeV/c, employing a modified version of the NA10 spectrometer. NA38 went further to record the first detection of charmonium production in relativistic heavy-ion collisions (138). A qualitatively new effect was found: The ratio $\sigma_{\psi'}/\sigma_{J/\psi}$ decreased by nearly a factor of two in S + U collisions with respect to the ratio in p + A collisions. The NA38 collaboration and its successor NA50 (37) have developed the capability to measure high-mass dimuon events in coincidence with event charge multiplicity and calorimetric transverse energy. They have recently recorded interesting data on J/ψ and ψ' production in Pb + Pb collisions at 157 GeV/c/nucleon [see review by Gerschel & Hüfner (139) in this volume].

The high-statistics experiment NA3 (134) confirmed observations by earlier experiments of large changes in the nuclear dependence as function of p_t and x_F. The NA3 nuclear dependence ratios versus x_F and p_t have similar shapes for beams of π^-, π^+, and protons, as shown in Figures 17 and 18.

Figures 19 and 20 compare proton-induced J/ψ production at 200 GeV/c and 800 GeV/c versus x_F and x_2. Figure 20 clearly demonstrates the lack of scaling with

[7]There are also significant nuclear effects in J/ψ production with real (135) and virtual photons (136). These are usually interpreted via the vector-dominance model in terms of J/ψ absorption on nucleons.

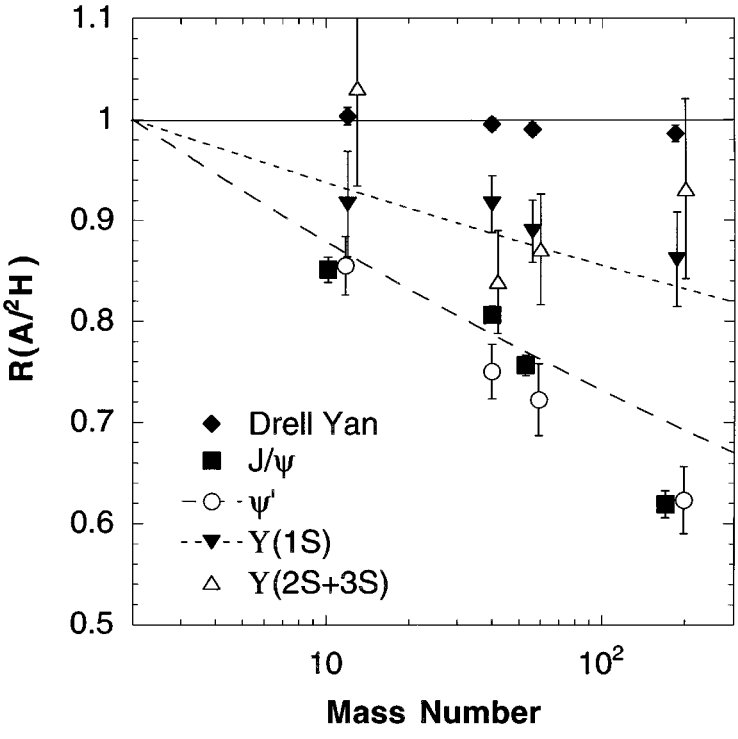

Figure 16 Ratios of heavy-nucleus to deuterium integrated yields per nucleon for 800 GeV/c proton production of dimuons from the Drell-Yan process and from decays of the J/ψ, ψ', $\Upsilon(1S)$, and $\Upsilon(2S + 3S)$ states (104). Short-dashed and long-dashed curves represent the approximate nuclear dependences for the $b\bar{b}$ and $c\bar{c}$ states, $A^{0.96}$ and $A^{0.92}$, respectively.

x_2. Such scaling would be expected for an effect whose origin was primarily due to a nuclear dependence of the target structure function—such as shadowing. In addition, even though the 800-GeV/c data are in the range where shadowing is expected, the observed nuclear dependence is much larger than expected for shadowing alone.

The nuclear dependence shows a rise when plotted against p_t for the J/ψ (Figure 18) and the Υ resonances. Table 2 lists $\Delta\langle p_t^2\rangle$ for J/ψ and Υ production. The NA3 values are from Badier et al (134). The E772 values (PL McGaughey, JM Moss, JC Peng, unpublished data) use a parameterization that reproduces $d\sigma/dp_t^2$ for the Υ data (10) on ^2H, and the p_t dependence of the ratio of cross sections $R(\sigma_A/\sigma_{2H})$. Unfortunately, the same analysis could not be performed for the E772's J/ψ data owing to the very limited acceptance in p_t.

The values of $\Delta\langle p_t^2\rangle$ are similar for the J/ψ and the Υ, albeit at different beam energies. The effect is three to four times larger for quarkonia than for DY production. A factor of two of this increase may be attributable to final-state multiple scattering, which is absent in the DY process.

TABLE 2 Values of $\Delta\langle p_t^2\rangle \equiv \langle p_t^2\rangle(A) - \langle p_t^2\rangle(^2\mathrm{H})$ for proton-induced production of the J/ψ and Υ resonances. E772 values were determined starting with a function, $d\sigma/dp_t^2 = C(1 + (p_t/p_0)^2)^{-6}$, with $p_0 = 2.8$ GeV/c, which fits the ^{2}H data for the Υ resonance. The NA3 value for the J/ψ uses ^{1}H rather than ^{2}H

Experiment	State	Beam	A	$\Delta\langle p_t^2\rangle$ (GeV^2/c^2)
NA3 (134)	J/ψ	200 GeV/c	W	0.34 ± 0.06
E772 (123)	Υ	800 GeV/c	C	$0.141 \pm 0.078 \pm 0.03$ (syst.)
			Ca	$0.200 \pm 0.041 \pm 0.03$ (syst.)
			Fe	$0.315 \pm 0.039 \pm 0.03$ (syst.)
			W	$0.410 \pm 0.078 \pm 0.03$ (syst.)

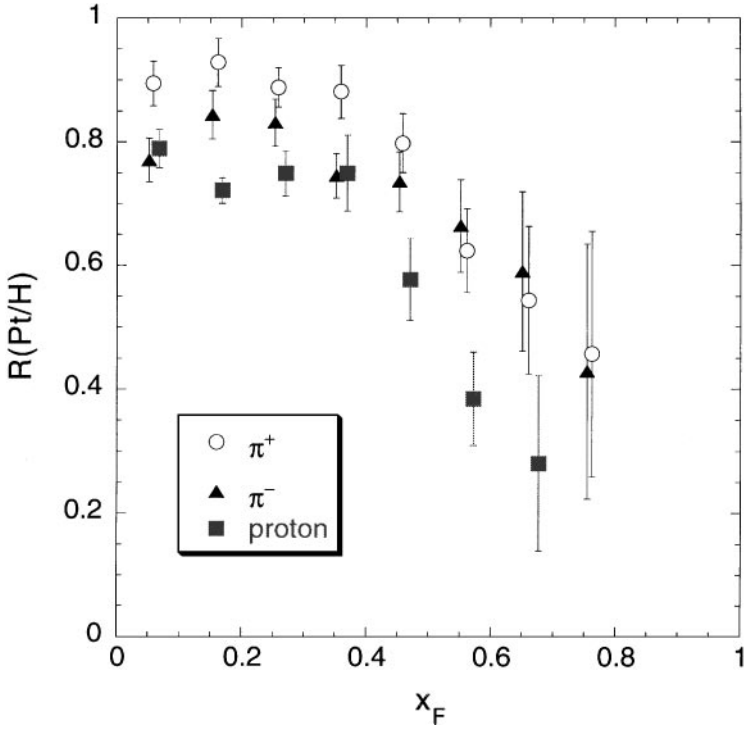

Figure 17 Ratios of J/ψ cross sections per nucleon, platinum over hydrogen, versus x_F for 200 GeV/c π^+, π^-, and proton data from experiment NA3 (134).

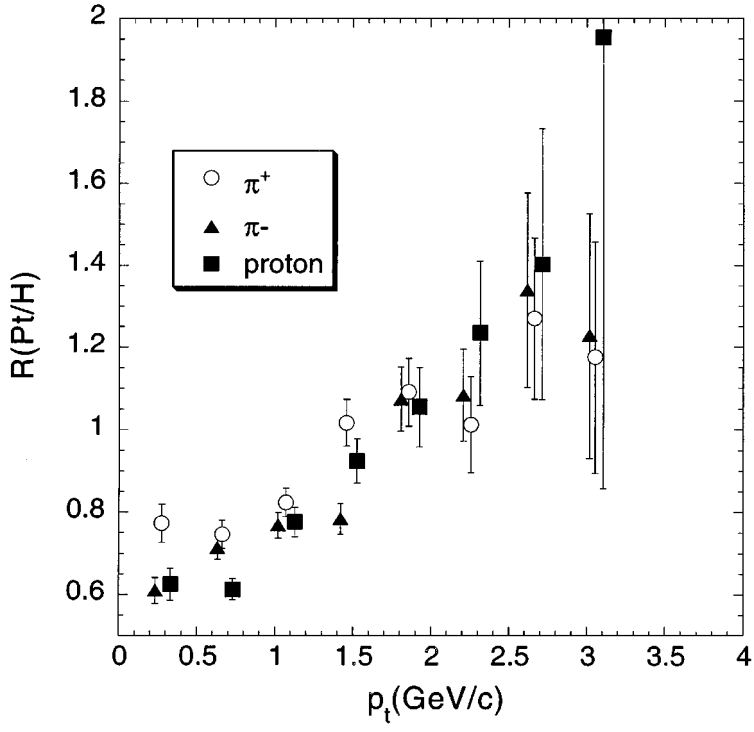

Figure 18 Ratios of J/ψ cross sections per nucleon, platinum over hydrogen, versus p_t for 200 GeV/c π^+, π^-, and proton data from experiment NA3 (134).

4.3 Nuclear Dependence of Open Charm Production

The nuclear dependence of open heavy flavor production is much more difficult to measure than that of DY or quarkonium production. Four experiments employing vertex detectors to identify D meson decays have determined values of α. As shown in Table 3, in contrast to J/ψ and ψ' production, there is no evidence of a nuclear dependence to open charm production at small x_F. No measurements have yet been made of the nuclear dependence of open beauty production.

TABLE 3 Nuclear dependence of open charm production via vertex-identified D meson decays

Experiment	Beam	$\langle x_F \rangle$	α
WA82 (140)	340 GeV/c π^-	0.24	0.92 ± 0.06
E769 (141)	250 GeV/c π^-	0.0	$1.0 \pm 0.05 \pm 0.02$
E789 (142)	800 GeV/c p	0.031	$1.02 \pm 0.03 \pm 0.02$
WA92 (143)	350 GeV/c π^-	0.18	$0.95 \pm 0.06 \pm 0.03$

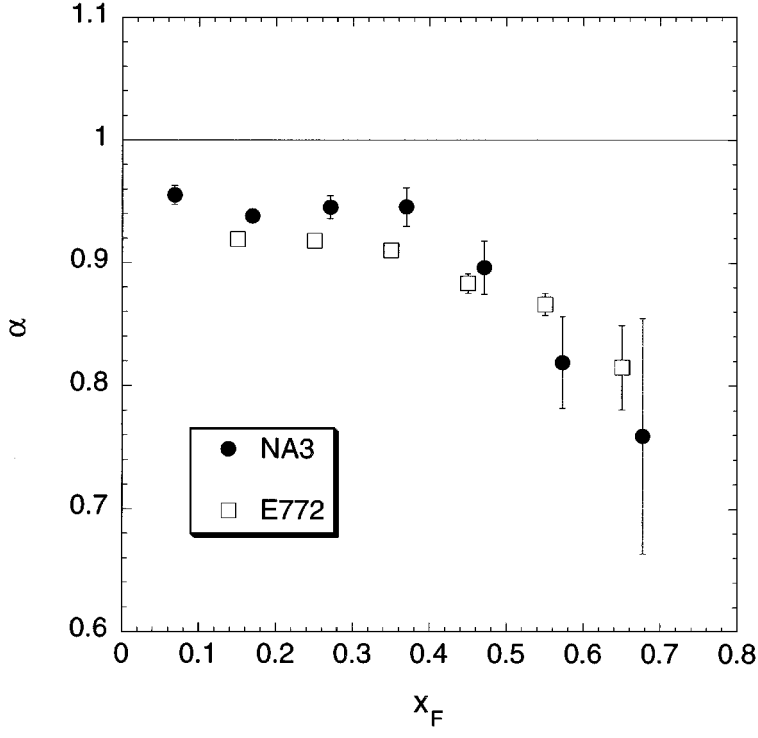

Figure 19 α versus x_F for proton-induced J/ψ production at 200 GeV/c (134) and 800 GeV/c (137).

4.4 Nuclear Effects in Quarkonium Production and the Quark-Gluon Plasma

Much of the interest in the nuclear dependence of quarkonium production is connected to the search for production of the QGP in collisions of relativistic heavy ions (see Gerschel & Hüfner (139), this volume). In brief, the concept put forth by Matsui & Satz (144) is that states such as the J/ψ and ψ' would not survive if a QGP were formed, since their radii exceed the effective $c\bar{c}$ screening length in the QGP. Thus, one should observe a suppression of these states in central collisions of heavy ions compared with proton-proton or proton-nucleus collisions (where the QGP is presumably not formed). The large nuclear effects found in proton-nucleus collisions complicate this simple picture. In recent years, much effort has been directed at refining the phenomenology of the Matsui-Satz effect in order to identify truly new physics that may be manifested in hot-dense matter occupying an extended volume (139).

To what extent are nuclear effects in quarkonium production understood? As skeptical experimentalists, we are tempted to respond, "Not very well." We do not attempt a detailed review of the numerous models on the market but rather

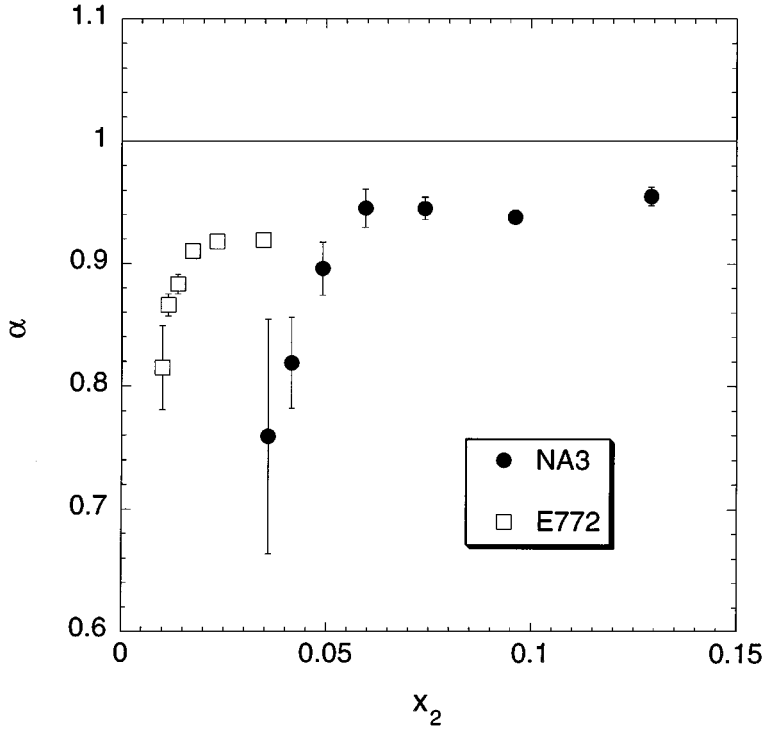

Figure 20 α versus x_2 for proton-induced J/ψ production at 200 GeV/c (134) and 800 GeV/c (137).

enumerate some of the basic experimental elements that must be addressed by models of quarkonium production in nuclear systems.

1. Significant nuclear effects are found in hadronic production of all heavy quarkonium states. Charm is more suppressed than beauty, but both exhibit nuclear dependences that are much larger than those found for the DY process at comparable values of Q^2. The few measurements of open charm production, based on vertex-identified decays of D mesons, exhibit no nuclear dependence.
2. The nuclear suppression for J/ψ and ψ' is the same, within errors, as it is for Υ and the sum of Υ' and Υ'' resonances. Thus, the effect does not depend on the final size of the hadron. It is important to appreciate that roughly half of the total production of the J/ψ originates in decays from higher states, including the ψ' (35).
3. The nuclear suppression becomes more pronounced at large x_F or small x_2. However, it does not scale with x_2. The nuclear dependence versus x_F is similar for production of the J/ψ with 200-GeV/c and 800-GeV/c protons.

4. A relative nuclear enhancement occurs at large p_t. Although this effect is also observed for DY production (104, 122), the rise with p_t is much larger for the quarkonium states. The interpretation of the p_t dependence in terms of parton energy loss (121) is more complicated than for DY production (Section 3.7) because both initial- and final-state effects can contribute.

Although there is now a considerable body of data, much uncertainty remains in the phenomenological description of quarkonium production in nuclei. New nuclear-dependence measurements at negative values of x_F would rank high as a discriminant between current competing models. Such measurements are difficult at fixed-target facilities, but it is hoped that they will be carried out in the early years of RHIC.

Hadronic production of quarkonium itself remains a field of intense theoretical interest (3). Many of the desirable new experimental investigations relating to the importance of color-octet production, e.g. measurements of polarization, would also have an immediate impact on issues related to nuclear dependence. Such measurements would also have a significant impact on the understanding of quarkonium suppression as a signature of the creation of the QGP.

5. FUTURE PROSPECTS

The next decade will see a qualitative change in experimental capability to study dilepton production in hadronic processes. Two new hadron colliders, RHIC and the Large Hadron Collider (LHC), will be in operation. Both will have the capability of accelerating and colliding a variety of beams—p + p, p + A, to A + A, where A can range to the heaviest nuclei. RHIC will operate in the range $50 < \sqrt{s} < 500$ GeV/nucleon. Starting in 2000, RHIC will also be able to collide polarized protons up to $\sqrt{s} = 500$ GeV. Although specific experimental capabilities are still being developed at these facilities, areas of new opportunity related to the subjects reviewed here can be readily identified.

No p + p collisions have been carried out above the energy range of the CERN intersecting storage rings. Thus, DY production at RHIC and LHC will produce new information for parton density distributions as well as for other issues in QCD that are accessible via this well-understood reaction. Extension of shadowing studies in hadronic processes requires the highest-energy p + A collisions. The DY and direct photon production are the most readily interpreted processes for such investigations. The DY process in central collisions of ultrarelativistic heavy ions is the most theoretically tractable of the QCD processes in this exceedingly complex dynamical system. Although DY production is expected to take place prior to the putative transition to the QGP, there may be surprises.

$W^{\pm}$ production in p + p collisions, a first for hadron colliders, will give a direct indication of the flavor asymmetry of the proton, not requiring the assumption of charge symmetry (145). Additionally, new tests of the validity of charge symmetry might be performed via reactions such as $p + d \rightarrow W^{\pm}$ (92; S Vigdor,

unpublished). As discussed in Section 3.2, polarized proton collisions offer a wealth of new opportunities for the delineation of different aspects of polarized parton structure. The enormous range of Q^2 spanned from DY to $W^{\pm}$ and Z^0 production will give a unique window for observing the interplay between quark and gluon spins.

RHIC and the heavy-ion program at the LHC are strongly focused on finding evidence of the QGP. A major element in this search will be quarkonium suppression. As we have seen, however, the origins of many strong nuclear effects observed in quarkonium production in p + A collisions remain mysterious. With the new capabilities of dilepton measurement in collider detectors, some of these mysteries may be investigated more easily than in closed-aperture fixed-target experiments.

The new 120-GeV/c Fermilab Main Injector (FMI), scheduled to begin operation in 2001, and the proposed 50-GeV/c Japanese Hadron Facility (146) present capabilities at the other end of the x scale. In contrast with the past 800-GeV/c fixed-target program at Fermilab, which could only operate in competition with the collider, the FMI program will run in parallel. Simple scaling rules show that large-x physics is often best carried out at comparatively low energies, where cross sections are largest. As we have seen, measurements of $\bar{d}/\bar{u}$ and the nuclear dependence of the antiquark sea at high x require beams from the FMI (147).

In conclusion, dilepton production in hadron-hadron interaction continues to be a very powerful tool for probing the parton structure of hadrons and nuclei and for studying the dynamics of the strong interactions. We expect significant progress in these areas for the foreseeable future, as the next generation of hadron colliders and high-intensity accelerators begins operation.

ACKNOWLEDGMENTS

We are grateful to our many collaborators on the E772, E789, and E866 experiments at Fermilab. In particular, we would like to acknowledge Chuck Brown, whose expert advice and assistance have been invaluable. This work was supported by the US Department of Energy, Nuclear Science Division, under contract W-7405-ENG-36.

LITERATURE CITED

1. Drell SD, Yan TM. *Phys. Rev. Lett.* 25:316 (1971)
2. Hawker EH, et al (E866 Collaboration). *Phys. Rev. Lett.* 80:3715 (1998)
3. Braaten E, Fleming S, Yuan TC. *Annu. Rev. Nucl. Part. Sci.* 46:197 (1996)
4. Kenyon IR. *Rep. Prog. Phys.* 45:1261 (1982)
5. Lyons L. *Prog. Part. Nucl. Phys.* 7:169 (1981)

6. Grosso-Pilcher C, Shochet M. *Annu. Rev. Nucl. Part. Sci.* 36:1 (1986)
7. Freudenreich K. *Int. J. Mod. Phys.* A5:3643 (1990)
8. Badier J, et al. *Z. Phys. C* 26:489 (1984)
9. Moreno G, et al. *Phys. Rev. D* 43:2815 (1991)
10. McGaughey PL, et al. *Phys. Rev. D* 50:3038 (1994)
11. Lai HL, et al. *Phys. Rev. D* 55:1280 (1997)
12. McGaughey PL. *Nucl. Phys.* A610:394c (1996)
13. Collins JC, Soper DE. *Phys. Rev. D* 16:2219 (1977)
14. Stirling WJ, Whalley MR. *J. Phys.* G19:D1 (1993)
15. Altarelli G, Ellis RK, Martinelli G. *Phys. Lett.* B151:457 (1985)
16. Rijken PJ, van Neerven WL. *Phys. Rev. D* 51:44 (1995)
17. Oakes RJ. *Nuovo Cim.* A44:440 (1966)
18. Collins JC. *Phys. Rev. Lett.* 42:291 (1979)
19. Chiappetta P, Le Bellac M. *Z. Phys. C* 32:521 (1986)
20. Lam CS, Tung WK. *Phys. Rev. D* 21:2712 (1980)
21. Guanziroli M, et al. *Z. Phys. C* 37:545 (1988)
22. Conway JS, et al. *Phys. Rev. D* 39:92 (1989)
23. Badier J, et al. *Z. Phys. C* 11:195 (1981)
24. Heinrich JG, et al. *Phys. Rev. D* 44:1909 (1991)
25. Berger EL, Brodsky SJ. *Phys. Rev. Lett.* 42:940 (1979)
26. Berger EL. *Z. Phys. C* 4:289 (1980)
27. Eskola KJ, et al. *Phys. Lett.* B333:526 (1994)
28. Brandenburg A, et al. *Phys. Rev. Lett.* 73: 939 (1994)
29. Collins JC, Soper DE. *Annu. Rev. Nucl. Part. Sci.* 37:383 (1987)
30. Sterman G, et al. *Rev. Mod. Phys.* 67:157 (1995)
31. Bodwin GT, Brodsky SJ, Lepage GP. *Phys. Rev. Lett.* 47:1799 (1981)
32. Collins JC, Soper DE, Sterman G. *Phys. Lett.* B134:263 (1984)
33. Bodwin GT. *Phys. Rev. D* 31:2616 (1985)
34. Kowitt MS, et al. *Phys. Rev. Lett.* 72:1318 (1994)
35. Antoniazzi L, et al. *Phys. Rev. Lett.* 70:383 (1993)
36. Anderson L, et al. *Nucl. Instrum. Methods* 223:23 (1984)
37. Abreu MC, et al. *Phys. Lett.* B410:337 (1997)
38. Baldit A, et al. *Phys. Lett.* B332:244 (1994)
39. Abromowicz H, et al. *Z. Phys. C* 15:19 (1982)
40. Gottfried K. *Phys. Rev. Lett.* 18:1174 (1967)
41. Stein S. *Phys. Rev. D* 12:1884 (1975)
42. Aubert JJ. *Nucl. Phys.* B293:740 (1987)
43. Benvenuti AC, et al. *Phys. Lett.* B237:599 (1990)
44. Field RD, Feynman RP. *Phys. Rev. D* 15: 2590 (1977)
45. Amaudruz P, et al. *Phys. Rev. Lett.* 66:2712 (1991); Arneodo M, et al. *Phys. Rev. D* 50:R1 (1994)
46. Martin AD, Stirling WJ, Roberts RG. *Phys. Lett.* B252:653 (1990)
47. Ellis SD, Stirling WJ. *Phys. Lett.* B256:258 (1991)
48. Ito AS, et al. *Phys. Rev. D* 23:604 (1981)
49. McGaughey PL, et al. *Phys. Rev. Lett.* 69: 1726 (1991)
50. Martin AD, Roberts RG, Stirling WJ. *Phys. Lett.* B387:419 (1996)
51. Peng JC, et al. *Phys. Rev. D* 58:092004 (1998)
52. Ackerstaff K, et al. *Phys. Rev. Lett.* 81:5519 (1998)
53. Martin AD, et al. *Eur. Phys. J.* C4:463 (1998)
54. Kumano S. *Phys. Rep.* 303:183 (1998)
55. Thomas AW. *Phys. Lett.* B126:97 (1983)
56. Sullivan JD. *Phys. Rev. D* 5:1732 (1972)
57. Henley EM, Miller GA. *Phys. Lett.* B251: 453 (1990)
58. Kumano S. *Phys. Rev. D* 43:3067 (1991); 43:59 (1991); Kumano S, Londergan JT. *Phys. Rev. D* 44:717 (1991)

59. Signal A, Schreiber AW, Thomas AW. *Mod. Phys. Lett.* A6:271 (1991)
60. Hwang WP, Speth J, Brown GE. *Z. Phys. A* 339:383 (1991)
61. Szczurek A, Speth J, Garvey GT. *Nucl. Phys.* A570:765 (1994)
62. Koepf W, Frankfurt LL, Strikman M. *Phys. Rev.* D53:2586 (1996)
63. Eichten EJ, Hinchliffe I, Quigg C. *Phys. Rev. D* 45:2269 (1992); 47:R747 (1993)
64. Cheng TP, Li LF. *Phys. Rev. Lett.* 74:2872 (1995)
65. Szczurek A, Buchmans A, Faessler A. *J. Phys.* C22:1741 (1996)
66. Cheng TP, Li LF. *Phys. Lett.* B366:365 (1996)
67. Ji X, Tang J. *Phys. Lett.* B362:182 (1995)
68. Brodsky SJ, Ma B. *Phys. Lett.* B381:317 (1996)
69. Bazarko AO, et al. *Z. Phys. C* 65:189 (1995)
70. Anselmino M, Efremov A, Leader E. *Phys. Rep.* 261:1 (1995); Erratum, 281:399 (1997)
71. Hughes E, Voss R. *Annu. Rev. Nucl. Part. Sci.* 49:303–39 (1999)
72. Close FE, Sivers D. *Phys. Rev. Lett.* 39: 1116 (1977)
73. Moss JM. *Int. Conf. Polarization Phenomena in Nucl. Phys., AIP Conf. Proc.* 339:721 (1994)
74. Ratcliffe P. *Nucl. Phys.* B223:45 (1983)
75. Gehrmann T. *Nucl. Phys.* B498:245 (1997)
76. Kamal B. *Phys. Rev. D* 57:6663 (1998)
77. Bourrely C, Soffer J. *Phys. Lett.* B314:132 (1993)
78. Ralston J, Soper DE. *Nucl. Phys.* B152:109 (1979)
79. Jaffe RL, Ji X. *Phys. Rev. Lett.* 67:552 (1991)
80. Bunce G, et al. *Part. World* 3:1 (1992)
81. Miller GA, Nefkens BMK, Slaus I. *Phys. Rep.* 194:1 (1990)
82. Henley EM, Miller GA. *Mesons in Nuclei*, ed. M Rho, DH Wilkinson. Amsterdam: North-Holland (1979)
83. Ma B. *Phys. Lett.* B274:111 (1992)
84. Ma B, Schäfer A, Greiner W. *Phys. Rev. D* 47:51 (1993)
85. Sather E. *Phys. Lett.* B274:433 (1992)
86. Londergan JT, et al. *Phys. Lett.* B340:115 (1994)
87. Rodionov EN, Thomas AW, Londergan JT. *Int. J. Mod. Phys. Lett.* A9:1799 (1994)
88. Benesh CJ, Goldman T. *Phys. Rev. C* 55: 441 (1997)
89. Benesh CJ, Londergan JT. *Phys. Rev. C* 58:1218 (1998)
90. Londergan JT, Thomas AW. *Progress in Particle and Nuclear Physics*, ed. A Faessler, 41:49. Amsterdam: Elsevier (1998)
91. Boros C, Londergan JT, Thomas AW. *Phys. Rev. Lett.* 81:4075 (1998)
92. Boros C, Londergan JT, Thomas AW. *Phys. Rev.* D 59:074021 (1999)
93. Betev B, et al. *Z. Phys. C* 28:9 (1985)
94. Freudenreich K. *Int. J. Mod. Phys.* A19: 3643 (1990)
95. Badier J, et al. *Z. Phys. C* 18:281 (1983)
96. Conway JS, et al. *Phys. Rev. D* 39:92 (1989)
97. Sutton PJ, et al. *Phys. Rev.* D45:2349 (1992)
98. Badier J, et al. *Phys. Lett.* B93:354 (1980)
99. Alberg M, et al. *Phys. Lett.* B389:367 (1996)
100. Alberg M, Falter T, Henley EM. *Nucl. Phys.* A644:93 (1998)
101. Aubert JJ, et al (EMC Collaboration). *Phys. Lett.* B123:295 (1983)
102. Geesaman DF, Saito K, Thomas AW. *Annu. Rev. Nucl. Part. Sci.* 45:337 (1995)
103. Amaudruz P, et al (NMC Collaboration). *Nucl. Phys.* B441:3 (1995)
104. Alde DA, et al (E772 Collaboration). *Phys. Rev. Lett.* 64:2479 (1990)
105. Ericson T, Weise W. *Pions in Nuclei*. Oxford, UK: Oxford Univ. Press (1987)
106. Friman BL, Pandharipande VR, Wiringa RB. *Phys. Rev. Lett.* 51:763 (1983)
107. Pandharipande VR, et al. *Phys. Rev. C* 49:789 (1994)
108. Benhar O, Pandharipande VR, Sick I. *Phys. Lett.* B410:79 (1997)

109. Akmal A, et al. *Phys. Rev. C* 56:2261 (1997)
110. Brown GE, et al. *Nucl. Phys.* A593:295 (1993)
111. Koltun DS. *Phys. Rev. C* 57:1210 (1998)
112. Kopeliovich BZ, Raufeisen J, Tarasov AV. *Phys. Lett.* B440:151 (1998)
113. Mueller AH, Qiu J. *Nucl. Phys.* B268:427 (1986); Qui J. *Nucl. Phys.* B291:749 (1987)
114. Gavin S, Milana J. *Phys. Rev. Lett.* 68:1834 (1992)
115. Frankel S, Frati W. *Phys. Rev. D* 51:4783 (1995)
116. Frankfurt LL, Strikman MI, Liuti S. *Phys. Rev. Lett.* 65:1725 (1990)
117. Bari G, et al. *Phys. Lett.* B163:282 (1985)
118. Brodsky SJ, Hoyer P. *Phys. Lett.* B298: 165 (1993)
119. Gyulassy M, Wang XN. *Nucl. Phys.* B429:583 (1994)
120. Luo M, Qui J, Sterman G. *Phys. Rev. D* 49:4493 (1994)
121. Baier R, et al. *Nucl. Phys.* B484:265 (1997); B531:403 (1998)
122. Bordalo P, et al. *Phys. Lett.* B193:373 (1987)
123. Alde DA, et al (E772 Collaboration). *Phys. Rev. Lett.* 66:2285 (1991)
124. Ashman J, et al. *Z. Phys. C* 52:1 (1991)
125. Ryan JJ, et al. *Proc. Meet. Am. Phys. Soc. Div. Particles and Fields, 7th*, ed. CH Albright, et al, p. 929. Singapore: World Sci. (1993)
126. Naples D, et al. *Proc. Meet. Am. Phys. Soc. Div. Particles and Fields, 7th*, ed. CH Albright, et al, p. 948. Singapore: World Sci. (1993)
127. Sansoni A, et al (CDF Collaboration). *Nuovo Cim.* A109:827 (1996)
128. Beneke M, Rothstein IZ. *Phys. Rev. D* 54:7082 (1996)
129. Tang W-K, Vänttinen M. *Phys. Rev. D* 54:4349 (1996)
130. Schuler GA, Vogt R. *Phys. Lett.* B387:181 (1996)
131. Antipov TM, et al. *Phys. Lett.* B76:235 (1978)
132. Anderson KJ, et al. *Phys. Rev. Lett.* 42:944 (1979)
133. Corden MJ, et al. *Phys. Lett.* B110:415 (1982)
134. Badier J, et al. *Z. Phys. C* 20:101 (1983)
135. Sokoloff MD, et al. *Phys. Rev. Lett.* 15: 3003 (1986)
136. Arneodo M, et al. *Phys. Lett.* B332:195 (1994)
137. Alde DA, et al (E772 Collaboration). *Phys. Rev. Lett.* 66:133 (1991)
138. Baglin C, et al. *Phys. Lett.* B345:617 (1995)
139. Gerschel C, Hüfner J. *Annu. Rev. Nucl. Part. Sci.* 49:255–301 (1999)
140. Adamovich M, et al. *Phys. Lett.* B284:453 (1992)
141. Alves GA, et al. *Phys. Rev. Lett.* 70:722 (1993)
142. Leitch MJ, et al. *Phys. Rev. Lett.* 72:2542 (1994)
143. Adamovich M, et al. *Nucl. Phys.* B495:3 (1997)
144. Matsui T, Satz H. *Phys. Lett.* B178:416 (1986)
145. Peng JC, Jansen DM. *Phys. Lett.* B354: 460 (1995)
146. JHF Project Office. *Proposal for Japan Hadron Facility*, KEK Rep. 97-3 (1997)
147. Geesaman D, et al. *Fermilab Proposal P906* (1999)

Annual Review of Nuclear and Particle Science
Volume 49, 1999

CONTENTS